

This is a repository copy of *Parallel adaptation of rabbit populations to myxoma virus*.

White Rose Research Online URL for this paper:

<https://eprints.whiterose.ac.uk/143315/>

Version: Accepted Version

---

**Article:**

Alves, Joel M., Carneiro, Miguel, Cheng, Jade Y. et al. (25 more authors) (2019) Parallel adaptation of rabbit populations to myxoma virus. Science. ISSN 0036-8075

<https://doi.org/10.1126/science.aau7285>

---

**Reuse**

Items deposited in White Rose Research Online are protected by copyright, with all rights reserved unless indicated otherwise. They may be downloaded and/or printed for private study, or other acts as permitted by national copyright laws. The publisher or other rights holders may allow further reproduction and re-use of the full text version. This is indicated by the licence information on the White Rose Research Online record for the item.

**Takedown**

If you consider content in White Rose Research Online to be in breach of UK law, please notify us by emailing [eprints@whiterose.ac.uk](mailto:eprints@whiterose.ac.uk) including the URL of the record and the reason for the withdrawal request.

# **Title: Parallel adaptation of rabbit populations to myxoma virus**

**Authors:** Joel M. Alves<sup>1,2,3\*</sup>, Miguel Carneiro<sup>2,4\*</sup>, Jade Y. Cheng<sup>5,6</sup>, Ana Lemos de Matos<sup>7</sup>, Masmudur M. Rahman<sup>7</sup>, Liisa Loog<sup>3,8</sup>, Paula F. Campos<sup>6,9</sup>, Nathan Wales<sup>6,10</sup>, Anders Eriksson<sup>11</sup>, Andrea Manica<sup>12</sup>, Tanja Strive<sup>13,14</sup>, Stephen C. Graham<sup>15</sup>, Sandra Afonso<sup>2</sup>, Diana J. Bell<sup>16</sup>, Laura Belmont<sup>7</sup>, Jonathan P. Day<sup>1</sup>, Susan J. Fuller<sup>17</sup>, Stéphane Marchandeu<sup>18</sup>, William J. Palmer<sup>19</sup>, Guillaume Queney<sup>20</sup>, Alison K. Surridge<sup>16</sup>, Filipe G. Vieira<sup>6</sup>, Grant McFadden<sup>7</sup>, Rasmus Nielsen<sup>5,6</sup>, M. Thomas P. Gilbert<sup>6,21</sup>, Pedro J. Esteves<sup>2,22</sup>, Nuno Ferrand<sup>2,4,23</sup>, Francis M. Jiggins<sup>1\*</sup>

\*Correspondence to [joel.alves@arch.ox.ac.uk](mailto:joel.alves@arch.ox.ac.uk), [miguel.carneiro@cibio.up.pt](mailto:miguel.carneiro@cibio.up.pt), [fmj1001@cam.ac.uk](mailto:fmj1001@cam.ac.uk)

## **Affiliations:**

<sup>1</sup>Department of Genetics, University of Cambridge, Cambridge, CB2 3EH, UK.

<sup>2</sup>CIBIO, Centro de Investigação em Biodiversidade e Recursos Genéticos, InBIO Laboratório Associado, Universidade do Porto, 4485-661 Vairão, Portugal.

<sup>3</sup>Palaeogenomics & Bio-Archaeology Research Network Research Laboratory for Archaeology and History of Art, University of Oxford, Dyson Perrins Building, South Parks Road, Oxford OX1 3QY, UK.

<sup>4</sup>Departamento de Biologia, Faculdade de Ciências da Universidade do Porto, 4169-007 Porto, Portugal.

<sup>5</sup>Departments of Integrative Biology and Statistics, University of California, Berkeley, Berkeley, CA 94720, USA.

<sup>6</sup>Centre for GeoGenetics, Natural History Museum of Denmark, University of Copenhagen, Copenhagen 1350, Denmark.

<sup>7</sup>The Biodesign Institute, Center for Immunotherapy, Vaccines, and Virotherapy, Arizona State University, Tempe, AZ 85287-5401, USA.

<sup>8</sup>Manchester Institute of Biotechnology, School of Earth and Environmental Sciences, University of Manchester, Manchester M1 7DN, UK.

<sup>9</sup>CIIMAR, Interdisciplinary Centre of Marine and Environmental Research, University of Porto, Avenida General Norton de Matos, S/N, 4450-208 Matosinhos, Portugal.

<sup>10</sup>Department of Plant and Microbial Biology, University of California, 111 Koshland Hall, Berkeley, CA 94720, USA.

<sup>11</sup>Department of Medical and Molecular Genetics, King's College London, London SE1 9RT, UK.

<sup>12</sup>Department of Zoology, University of Cambridge, Downing Street, Cambridge CB2 3EJ, UK.

<sup>13</sup>Health and Biosecurity, Commonwealth Scientific and Industrial Research Organisation, Canberra, ACT 2601, Australia.

<sup>14</sup>Centre for Invasive Species Solutions, University of Canberra, Bruce, ACT 2601,

45 Australia.

46 <sup>15</sup>Department of Pathology, University of Cambridge, Cambridge, CB2 1QP, UK.

47 <sup>16</sup>Centre for Ecology, Evolution and Conservation, School of Biological Sciences,  
48 University of East Anglia, Norwich NR4 7TJ, UK.

49 <sup>17</sup>School of Earth, Environmental and Biological Sciences, Science and Engineering  
50 Faculty, Queensland University of Technology, Brisbane, Australia.

51 <sup>18</sup>Office National de la Chasse et de la Faune Sauvage, Nantes, France.

52 <sup>19</sup>The Genome Center and Department of Plant Sciences, University of California,  
53 Davis, USA.

54 <sup>20</sup>ANTAGENE, Wildlife Genetics Laboratory, La Tour de Salvagny (Lyon), France.

55 <sup>21</sup>Norwegian University of Science and Technology, University Museum, 7491  
56 Trondheim, Norway.

57 <sup>22</sup>Instituto de Investigação e Formação Avançada em Ciências e Tecnologias da Saúde  
58 (CESPU), Gandra, Portugal.

59 <sup>23</sup>Department of Zoology, Faculty of Sciences, University of Johannesburg, Auckland  
60 Park 2006, South Africa.

61

62   **Abstract:** In the 1950s the myxoma virus was released into European rabbit  
63   populations in Australia and Europe, decimating populations and resulting in the rapid  
64   evolution of resistance. We investigated the genetic basis of resistance by comparing  
65   the exomes of rabbits collected before and after the pandemic. We found a strong  
66   pattern of parallel evolution, with selection on standing genetic variation favouring  
67   the same alleles in Australia, France and the United Kingdom. Many of these changes  
68   occurred in immunity-related genes, supporting a polygenic basis of resistance. We  
69   experimentally validated the role of several genes in viral replication and showed that  
70   selection acting on an interferon protein has increased its antiviral effect.

71 **Main Text:** The emergence of new infectious diseases can result in intense selective  
72 pressures on populations and cause rapid evolutionary change in both host and  
73 parasite. While pathogens must adapt to a new ecology and cellular environment,  
74 hosts can rapidly evolve resistance in a continuous arms-race. One of the most  
75 emblematic examples of this coevolutionary process arose when the wild European  
76 rabbit (*Oryctolagus cuniculus*) populations in Australia and Europe were exposed for  
77 the first time to the myxoma virus (MYXV; genus *Leporipoxvirus*, family  
78 *Poxviridae*). MYXV circulates naturally in American cottontail rabbits (*Sylvilagus*  
79 *spp.*) where it causes benign skin tumours, but in European rabbits it causes the highly  
80 lethal systemic disease myxomatosis (1).

81 Rabbits were initially introduced into Australia by European settlers, resulting in  
82 extensive ecological and economic damage (2). In an attempt to control the rabbit  
83 populations, MYXV was released in 1950 in Australia, after which it spread rapidly  
84 across the country, causing massive population reductions (1). In 1952 it was released  
85 in France and in 1953 it reached the United Kingdom (UK) with similar outcomes (2).  
86 In a series of classic experiments, the evolution of the virus and rabbits was tracked,  
87 and in all three countries substantial declines in case fatality rates in wild rabbits were  
88 observed both due to evolution of less virulent viral phenotypes and increased  
89 resistance in rabbit populations (3-5). Considered “one of the greatest natural  
90 experiments in evolution”, these observations ultimately became a textbook example  
91 of host-parasite coevolution (2).

92 Sixty-nine years have passed since myxomatosis was first released in Australia and  
93 today the virus continues to evolve in an ongoing arms-race against the rabbit immune  
94 system (6, 7). Despite much research on the genetics of MYXV, little is known about

the genetic basis of resistance to myxomatosis. The intense selective pressure exerted by the disease in rabbits and the parallel phenotypic evolution across multiple populations, provides an exceptional framework to study the evolution of resistance to a highly lethal pandemic in natural host populations. To understand the genetic basis of these changes we focused on three countries where genetic resistance independently emerged: Australia, France and the UK. For each one, we compared modern rabbits with historical specimens from museums that were collected before or soon after the release of the virus (1856-1956; Figs. 1 and S1, File S1).

### **Colonisation route of rabbits**

To obtain genome-wide polymorphism data we used oligonucleotide probes to capture 32.10Mb (1.17%) of the rabbit genome that includes the exome (19,293 genes), the mitochondrial genome, and three genomic regions that contain the Major Histocompatibility Complex region (MHC) encompassing 1.75 Mb. We sequenced 152 rabbits from Australia (historical:  $n=17$ , modern:  $n=26$ ), France (historical:  $n=29$ , modern:  $n=26$ ) and the UK (historical:  $n=29$ , modern:  $n=25$ ). The mean sequence coverage on-target per individual after filtering was 33X. After filtering, the number of bi-allelic SNPs was 757,333.

Historical records support the introduction of rabbits to the UK mainland from continental Europe by the 13<sup>th</sup> century (8) and most Australian rabbits are thought to be derived from an introduction in 1859 from the UK (9) (Fig. 1). Our genetic data reflects these historical records. Both Principal Components Analysis (PCA; Fig. 2a) and structure analyses (Fig. 2b;  $K=3$ ) reveal three clusters composed of individuals from the same country. The sequential colonisation from France to the UK and then Australia is reflected in the levels of genetic differentiation which are greatest

between France and Australia, and lowest between UK and Australia (Table S1). This pattern is repeated with the Australian populations clustering together with the UK in the structure analysis (Fig. 2b;  $K=2$ ). Population bottlenecks during colonisation can reduce genetic diversity and increase linkage disequilibrium (LD). Both aspects are reflected in the successive increases in LD (Fig. 2c) and decreases in heterozygosity (Fig. 2d) as rabbits moved from continental Europe to the UK and then Australia.

### **Genetic variation in historical and modern populations**

To detect changes in allele frequency due to natural selection, it is important that the genome-wide allele frequencies in our modern and historical samples are similar. Although changes in allele frequency are an expected signal of selection, artefactual variation generated by DNA degradation can generate similar signals between modern and historical DNA. To mitigate this, we sequenced samples to a high coverage, corrected for the effects of DNA damage patterns, and used a stringent set of filters at read and variant level. Genome-wide differences in allele frequency between our modern and historical samples could also arise due to population substructure. To minimise this effect, we sampled modern rabbits from locations near to where the historical specimens had been sampled (Figs. 1 and S1).

We consistently found that historical and modern populations from the same country exhibit similar patterns of genetic structure and diversity. In the PCA, the 95% confidence ellipses for historical and modern samples from the same country are interspersed (Fig. 2a). In the structure analysis, the patterns again reflect geography rather than the time of sampling (Fig. 2b,  $K=3$ ), and increasing the number of ancestral populations ( $K$ ) reveals finer population substructure instead of a split between the different time points (Fig. S2). More generally, across all SNPs the allele

frequencies of historical and modern populations are highly correlated in the three countries (Fig. 2e).

The collapse of populations due to myxomatosis has not increased levels of LD or decreased genetic diversity as both these parameters are similar between historical and modern populations (Figs. 2c and 2d). This is to be expected as the effective population size of rabbits is  $\sim 10^6$  (10), which is large for a vertebrate. Therefore, even if an  $\sim 99\%$  reduction in population size (as seen in some populations immediately after the first epidemic (6)), had been sustained for the subsequent 65 generations, the expected reduction in heterozygosity would have only been 0.35% (per generation reduction heterozygosity =  $1 - 1/(2N_e)$ ). Similarly, bottlenecks of this size are expected to have little effect on LD (11). Together, these results demonstrate that historical and modern samples are drawn from genetically similar populations. This strong correlation in allele frequencies between the two time points within each country is conducive to the identification of unusual shifts in allele frequency resulting from natural selection.

### **Parallel changes in allele frequency**

With a 99.8% case fatality rate of the originally released strain of MYXV, the myxomatosis pandemic imposed intense selection on rabbits, resulting in rapid and parallel evolution of increased resistance in exposed populations (6). To investigate whether parallel genetic changes occurred in Australia, France and the UK, we calculated  $F_{ST}$  between the historical and modern samples for each country and identified the 1000 SNPs that show the highest  $F_{ST}$ . By intersecting these three lists we found that more alleles have changed in frequency across two or three countries than expected by chance (Fig. 3a; File S2). Furthermore, considering the 92 SNPs in



the intersections of Fig. 3a, in 87 cases it was the same allele that had increased in frequency in the countries involved. It is particularly striking that SNPs that were among the top 1000 most differentiated in any two populations tend to show elevated  $F_{ST}$  in the third population (Fig. 3b). These results demonstrate the occurrence of parallel changes in allele frequency across the three populations.

To locate the putative targets of selection in the genome, we searched for SNPs that experienced large changes in allele frequency since the release of the MYXV. We accounted for the effects of population structure by scanning for outliers where the difference in allele frequency between modern and historical populations was larger than expected given the covariance matrix describing the joint allelic frequencies among populations inferred from the structure analysis (Fig. 2b,  $K=3$ ). In each population, we assumed selection started in the year the virus was introduced. For each SNP, we then compared the likelihood of a model where the change in allele frequency followed that predicted from the genome-wide amount of genetic drift across all historical and modern samples to a model that allowed additional changes in allele frequency through time (Fig. S3). Combining data across the three populations and allowing the strength of selection to vary independently in the three countries, we identified 193 SNPs in 98 genes and 7 intergenic regions that experienced significant changes in allele frequency (genome-wide significance  $p<0.05$ ; Fig. 3c; File S3. The results were similar when we assumed the same strength of in all countries (Fig. S4; File S3).

To explicitly test for parallel evolution and identify variants that significantly changed in frequency in all three populations, we compared the likelihood of our previous model, that assumed the equal selection across the three populations, to a model

where we allowed the alleles to change in frequency due to selection in one population only. We identified 94 SNPs that had a significant signature of parallel selection (genome-wide significance  $p < 0.05$ ; Fig. 3d, positive values).

It is common to find considerable standing genetic variation in susceptibility to infection within populations (12, 13), which may allow populations to rapidly evolve resistance when they encounter novel pathogens (14). This can be explicitly tested with our experimental design that incorporated historical samples. We found that in the large majority of cases, the SNPs under selection were also present in at least one of our historical populations (93% and 84% of the SNPs with a genome-wide  $P < 0.05$  in Figs. 3c and 3d, respectively). Therefore, parallel evolution has occurred because natural selection has been acting on standing genetic variation that was present over 800 years ago in continental Europe, and was carried with rabbits to the UK and Australia. The existence of this variation likely explains the rapid development of resistance to myxomatosis observed almost immediately after the first outbreaks.

### **Population-specific evolution**

Despite the common selection pressure imposed by myxomatosis, the populations of France, UK and Australia will have experienced their unique selection pressures, as resistance was evolving in a different ecological and genetic background. We can identify SNPs that have experienced population-specific changes in allele frequency from our previous analysis when the model of selection in one population is preferred over the model of selection in all three populations (negative values in Fig. 3d).

To quantify the proportion of SNPs under parallel or population-specific selection we used a Bayesian approach. First, we analysed data from each population

independently to identify variants under selection (Fig. S5, File S4; genome-wide  $p < 0.05$ ). This minimises the inherent bias towards detecting SNPs under parallel selection that occurs when the all populations are combined (Figs. 3c and 3d). We then returned to the combined dataset, and for each of the SNPs that were significant in the single population analysis we calculated a Bayes factor to compare models of population-specific versus parallel selection (Fig. S5). For each gene we retained only the most significant SNP ( $n=43$ , File S5). We found evidence that 20 SNPs were under population-specific and 20 were under parallel selection (for 3 SNPs we could not distinguish the models), implying that a large component of the recent selection in the three populations has occurred on a common set of variants.

Due to population bottlenecks as rabbits colonised new areas (Figs. 2c and 2d), alleles selected in one population may be rare or missing in other populations. This means that population-specific adaptation could result not just from differences in selection pressures but also due to differences in the variants available for selection to act on. To test this, we examined the frequency of the 20 alleles under population-specific selection in our historical samples. There were no consistent differences in the ancestral allele frequencies between the populations where we detected the effects of selection and populations where we did not (Table S2). Therefore, we can conclude that population-specific changes in allele frequency result from population-specific selection pressures, perhaps due to differences in ecology, genetic background or independent paths of co-evolution with MYXV (15).

### **Changes in the strength of selection**

The proportion of rabbits killed by myxomatosis has fallen since the 1950s, due to declines in the virulence of the virus and increases in resistance (6). Therefore, the

strength of selection on variants that confer resistance to MYXV is expected to have declined. However, in 1984 a new lethal viral pathogen was identified in rabbits, the rabbit haemorrhagic disease virus (RHDV; genus *Lagovirus*, family *Caliciviridae*) (16). RHDV, which has a similar case-fatality rate to myxomatosis, was first found in domestic rabbits in China, from where it spread to continental Europe in 1986, the UK in 1992 and Australia in 1995 (2, 17, 18). Like myxomatosis, RHDV caused high mortality across the two continents, which could have contributed to the observed changes in allele frequency.

To evaluate the role of RHDV in our selection signatures and understand how the strength of selection has changed through time, we obtained 70 rabbit samples that were collected before or soon after RHDV between 1985 and 1996, in the UK and Australia (Fig. 3e: File S1). We selected four SNPs that had experienced significant changes in allele frequency since the 1950s and that were located in or near genes with known immune functions (*CD96*, *FCRL3*, *IFN- $\alpha$ 21A* and MHC Class I), and genotyped them in these samples by Sanger sequencing. Combining these genotypes with data from our exome sequences, we used a Bayesian approach (19) to estimate the selection coefficient acting on these SNPs. We allowed two phases of selection. The first from when MYXV was released to the appearance of RHDV, and the second from the appearance of RHDV to the present day (Fig. 3e; note the date when the strength of selection changes is fixed in the model).

We found that the strength of selection on *FCRL3* and *IFN- $\alpha$ 21A* has declined through time in both the UK and Australia (Fig. 3e, File S6). This is consistent with selection being driven by MYXV, whose case fatality rate has decreased since its release, and does not support a role for RHDV. Intriguingly, the data suggests that

these variants have been negatively selected in recent decades (Fig. 3e), which is predicted if they have negative pleiotropic costs on other fitness components. For *CD96* and MHC, there was no significant change in the strength of selection through time (File S6). Nonetheless, both the genes in the UK and *CD96* in Australia have a significant signal of positive selection before the release of RHDV.

We observed large changes in allele frequency across the two time periods (Fig. 3e). Averaging across populations during the first phase of selection, we estimate the per year selection coefficient was 0.16 for *IFN- $\alpha$ 21A*, 0.13 for *FCRL3*, 0.08 for *CD96* and 0.07 for MHC (File S6). These analyses assume the alleles were additive, but estimates of the timing and strength of selection remained similar if we assumed recessive or dominant mode of inheritance.

### **Selection on the immune system**

The innate immune response provides the first line of defence against viruses. It is activated by the secretion of cytokines including interferon- $\alpha$  (IFN- $\alpha$ ), which binds to receptors on uninfected neighbouring cells and induces an antiviral state. To circumvent this, MYXV encodes potent inhibitors of the interferon response, including the double-stranded RNA binding protein M029 (20, 21). Among the most significant increases in frequency in our dataset, there are three non-synonymous variants that segregate as a haplotype in the interferon- $\alpha$ 21A gene (*IFN- $\alpha$ 21A*; Fig. 3c). To evaluate the role of these SNPs in the antiviral activity of *IFN- $\alpha$ 21A*, we synthesised the two corresponding protein isoforms and tested their antiviral effect by measuring MYXV viral replication in a rabbit cell line. Neither isoform of IFN- $\alpha$ 21A affected the replication of the wild-type MYXV (Lausanne strain) (Fig. S6a), however both reduced significantly the replication of an attenuated strain of MYXV (M029

mutant) (22) (Figs. 4a and S6b). Moreover, we found that the isoform of IFN- $\alpha$ 21A (varIFN- $\alpha$ 21A) that had been favoured by selection more strongly inhibited the replication of M029 MYXV. This indicates that natural selection has increased the potency of the interferon response in modern rabbit populations that have co-evolved with MYXV. The selected allele also had an antiviral effect on vesicular stomatitis virus (VSV), an RNA virus (Fig. 4b). This suggests a general increase in the protein's antiviral activity and it may be that selection by MYXV has increased resistance to other viruses, including RHDV. While this effect was not apparent with wild-type MYXV, this could be a limitation of the cell culture-based experiment, since *in vivo* innate immune responses involve the coordinated action of multiple cytokines across many tissues. In such circumstances, it is possible that the isoform of IFN- $\alpha$ 21A that has been favoured by selection may contribute to attenuating wild-type MYXV infection.

We found a strong population-specific signal of selection on a non-synonymous variant in *CD200-R*, which is the receptor for the negative regulator of innate immune responses CD200. The selected allele was not observed in any of the historical populations, but it increased to a frequency of 56% in the modern French population (Fig. 3d). The selected residue is part of the CD200 binding interface (23) (Fig. S7). Mutation of this site in the human protein does not prevent CD200 binding (24), but it may affect binding affinity in a quantitative way. Therefore, any effects of this variant may occur via modulation of the rabbit CD200:CD200R interaction.

Alongside the innate immune response, hosts mount an adaptive antiviral immune response mediated by MHC class I proteins. Polymorphisms in the peptide-binding region of MHC proteins affect the repertoire of peptides they can present and are

frequently associated with variation in susceptibility to infectious disease (25). We found multiple SNPs in the MHC region that have experienced positive selection across the three populations (Fig. 3c). However, the top hits in this region were located in an intergenic region of 35.7Kb between two MHC class I genes (grey shaded box; Fig. 3c). We failed to sequence the regions encoding the peptide-binding regions of these proteins for most individuals (either the sequence capture or read mapping failed). Therefore, the variants that have increased in frequency in the intergenic region may be in LD with variants in the protein coding sequence that affect susceptibility to MYXV.

Other immunity genes that exhibit parallel changes in frequency include four non-synonymous variants in *FCRL3* (Fc Receptor-Like 3), a cell surface receptor that inhibits the activation of B cells (26). Three highly significant non-synonymous variants are in *CD96* which is a transmembrane receptor of T and NK cells involved in modulating immune responses (27, 28). The four SNPs with the highest likelihood in the entire dataset were all intronic variants present in the *MFSD1*, which encodes a transmembrane protein in the major facilitator superfamily. Several paralogs of this gene have been identified in a genome-wide RNAi screen for genes affecting replication of vaccinia virus, a poxvirus related to MYXV (29). Using RNAi, we found that this gene also modulated MYXV titres in rabbit cells (Fig. S6e).

### **Selection on proviral genes**

Resistance to viruses can evolve not only through improvement of antiviral defences, but also through changes in host proviral proteins that viruses hijack for their own benefit. Among our significant associations was a SNP in the 3' prime UTR of *VPS4* (Fig. 3c). This gene has no known role in the replication cycle of poxviruses, but is

required for the envelopment of herpes simplex virus (HSV) in the cytoplasm (30). To evaluate the role of VPS4 in MYXV replication we took advantage of a human cell line expressing a dominant-negative form of the VPS4 protein (30). By comparing the effect of MYXV in wild-type and VPS4 dominant-negative human cell lines, we found that the latter strongly inhibited MYXV replication (Figs. 4c, 4d, S6c and S6d). In contrast to HSV, the effect at a high multiplicity of infection suggests VPS4 may affect earlier replication steps in MYXV. Therefore, the VPS4 protein is proviral, and it is possible that selection by MYXV may have altered its expression in the modern rabbit populations.

The proteasome is required both for poxvirus uncoating after the cell entry (31) and the processing of antigenic peptides, and three variants in the gene *PSMG3* (pac3, proteasome assembly chaperone 3) increased 83% in frequency in France, with smaller changes in other populations. Using Sanger sequencing we found that these SNPs were associated with a 7-base pair insertion in the first exon and a 50-base pair deletion spanning the first intron and second exon. However, since genome annotation of this gene is incomplete the importance of these changes is unclear.

**Conclusions:** The myxomatosis pandemic caused massive mortality in rabbit populations, leading to the evolution of genetic resistance to the disease in Australia, France and the UK. We have found that over the last 60 years, the convergent phenotype of viral resistance in these populations was also accompanied by parallel genetic changes. This was a consequence of natural selection acting on standing genetic variation that was present in the ancestral rabbit populations in continental Europe and was retained in the subsequent colonisation process of the UK and Australia. The presence of this variation likely explains the rapid development of



resistance to myxomatosis observed in rabbit populations almost immediately after the first outbreaks and may frequently be critical to allow populations to respond to novel pathogens. This is in striking contrast to the evolution of the virus where parallel changes in MYXV virulence do not have a common genetic basis (15).

Despite rapid phenotypic evolution, only 1% of the alleles favoured by selection have reached fixation in any of the modern populations (Fig. 3c, 3 out of 193 SNPs).

Together with our estimates of selection coefficients and the moderate antiviral effect of the three interferon SNPs, this suggests genetic resistance to myxomatosis is a polygenic trait resulting from the cumulative effect of multiple alleles shifting in frequency across the genome, as opposed to a few major-effect changes to the immune response. Such adaptation is likely to result in a gradual ‘quantitative’ increase in resistance. When resistance reduces the within-host replication rate of the virus rather than completely preventing infection, selection will favour increases in viral virulence (32). Consistent with this prediction, it has recently been observed in wild populations of rabbits that the decline in virulence seen in the years immediately after the virus was released has been reversed and highly virulent viral genotypes have emerged (7).

The evolution of resistance to MYXV is associated with enhanced innate antiviral immunity (6). Homologs of CD96, FCRL, CD200-R and IFN- $\alpha$  all play a regulatory role in the innate immune response, including effects on lymphocyte proliferation and activation (21, 26, 27, 33). The increased virulence seen in recent MYXV isolates is associated with the virus becoming extremely immunosuppressive, causing the loss of cellular inflammatory responses, lymphocytes and neutrophils (7). Therefore, viral evolution may have found ways to counter the effect of many of the genetic

382 adaptations that we have observed. In conclusion, our results reveal how standing  
383 genetic variation in the immune system allowed populations to rapidly evolve  
384 resistance to a novel and highly virulent pathogen and describe the molecular and  
385 genetic basis of an iconic example of natural selection.

## References and Notes:

1. F. Fenner, F. N. Ratcliffe, *Myxomatosis* (Cambridge University Press, Cambridge ; New York, 1965).
2. F. Fenner, B. Fantini, *Biological Control of Vertebrate Pests: The History of Myxomatosis - an Experiment in Evolution*. (CABI publishing, New York, NY, USA, 1999).
3. J. Ross, M. F. Sanders, The development of genetic resistance to myxomatosis in wild rabbits in Britain. *J Hyg (Lond)*. **92**, 255–261 (1984).
4. F. Fenner, J. Ross, in *The European rabbit: The History and Biology of a Successful Colonizer*, H. V. Thompson, C. M. King, Eds. (Oxford University Press, Oxford ; New York, 1994), pp. 205–239.
5. I. D. Marshall, F. Fenner, Studies in the epidemiology of infectious myxomatosis of rabbits. V. Changes in the innate resistance of Australian wild rabbits exposed to myxomatosis. *J Hyg (Lond)*. **56**, 288–302 (1958).
6. P. J. Kerr, Myxomatosis in Australia and Europe: a model for emerging infectious diseases. *Antiviral Res.* **93**, 387–415 (2012).
7. P. J. Kerr *et al.*, Next step in the ongoing arms race between myxoma virus and wild rabbits in Australia is a novel disease phenotype. *Proc Natl Acad Sci USA*. **114**, 9397–9402 (2017).
8. E. M. Veale, The Rabbit in England. *Agric Hist Rev.* **5**, 85–90 (1957).
9. K. Myers, I. Parer, P. Wood, B. D. Cooke, in *The European rabbit: The History and Biology of a Successful Colonizer*, H. V. Thompson, C. M. King, Eds. (Oxford University Press, Oxford ; New York, 1994), pp. 108–157.
10. M. Carneiro, N. Ferrand, M. W. Nachman, Recombination and speciation: loci near centromeres are more differentiated than loci near telomeres between subspecies of the European rabbit (*Oryctolagus cuniculus*). *Genetics*. **181**, 593–606 (2009).
11. L. Kruglyak, Prospects for whole-genome linkage disequilibrium mapping of common disease genes. *Nat Genet.* **22**, 139–144 (1999).
12. A. V. S. Hill, Evolution, revolution and heresy in the genetics of infectious disease susceptibility. *Phil. Trans. R. Soc. B.* **367**, 840–849 (2012).
13. M. M. Magwire *et al.*, Genome-wide association studies reveal a simple genetic basis of resistance to naturally coevolving viruses in *Drosophila melanogaster*. *PLoS Genet.* **8**, e1003057 (2012).
14. J. C. Stephens *et al.*, Dating the origin of the CCR5-Delta32 AIDS-resistance allele by the coalescence of haplotypes. *Am. J. Hum. Genet.* **62**, 1507–1515 (1998).

- 424 15. P. J. Kerr *et al.*, Evolutionary history and attenuation of myxoma virus on two  
425 continents. *PLoS Pathog.* **8**, e1002950 (2012).
- 426 16. J. Abrantes, W. van der Loo, J. Le Pendu, P. J. Esteves, Rabbit haemorrhagic  
427 disease (RHD) and rabbit haemorrhagic disease virus (RHDV): a review. *Vet*  
428 *Res.* **43**, 12 (2012).
- 429 17. H. E. Fuller, D. Chasey, M. H. Lucas, J. C. Gibbens, Rabbit haemorrhagic  
430 disease in the United Kingdom. *Vet. Rec.* **133**, 611–613 (1993).
- 431 18. J. P. Morisse, G. Le Gall, E. Boilletot, Hepatitis of viral origin in Leporidae:  
432 introduction and aetiological hypotheses. *Rev Sci Tech.* **10**, 269–310 (1991).
- 433 19. L. Loog *et al.*, Inferring Allele Frequency Trajectories from Ancient DNA  
434 Indicates That Selection on a Chicken Gene Coincided with Changes in  
435 Medieval Husbandry Practices. *Mol Biol Evol.* **34**, 1981–1990 (2017).
- 436 20. G. L. Smith, J. A. Symons, A. Alcamí, Poxviruses: interfering with interferon.  
437 *Semin Immunol.* **8**, 409–418 (1998).
- 438 21. C. Upton, K. Mossman, G. McFadden, Encoding of a homolog of the IFN-  
439 gamma receptor by myxoma virus. *Science.* **258**, 1369–1372 (1992).
- 440 22. M. M. Rahman, J. Liu, W. M. Chan, S. Rothenburg, G. McFadden, Myxoma  
441 virus protein M029 is a dual function immunomodulator that inhibits PKR and  
442 also conscripts RHA/DHX9 to promote expanded host tropism and viral  
443 replication. *PLoS Pathog.* **9**, e1003465 (2013).
- 444 23. D. Hatherley, S. M. Lea, S. Johnson, A. N. Barclay, Structures of  
445 CD200/CD200 receptor family and implications for topology, regulation, and  
446 evolution. *Structure.* **21**, 820–832 (2013).
- 447 24. D. Hatherley, A. N. Barclay, The CD200 and CD200 receptor cell surface  
448 proteins interact through their N-terminal immunoglobulin-like domains. *Eur.*  
449 *J. Immunol.* **34**, 1688–1694 (2004).
- 450 25. A. L. Hughes, M. Yeager, Natural selection at major histocompatibility  
451 complex loci of vertebrates. *Annu. Rev. Genet.* **32**, 415–435 (1998).
- 452 26. Y. Kochi *et al.*, FCRL3, an autoimmune susceptibility gene, has inhibitory  
453 potential on B-cell receptor-mediated signaling. *J. Immunol.* **183**, 5502–5510  
454 (2009).
- 455 27. L. Martinet, M. J. Smyth, Balancing natural killer cell activation through paired  
456 receptors. *Nat. Rev. Immunol.* **15**, 243–254 (2015).
- 457 28. A. Fuchs, M. Colonna, The role of NK cell recognition of nectin and nectin-  
458 like proteins in tumor immunosurveillance. *Semin. Cancer Biol.* **16**, 359–366  
459 (2006).

- 460 29. G. Sivan *et al.*, Human genome-wide RNAi screen reveals a role for nuclear  
461 pore proteins in poxvirus morphogenesis. *Proc Natl Acad Sci USA*. **110**, 3519–  
462 3524 (2013).
- 463 30. C. M. Crump, C. Yates, T. Minson, Herpes simplex virus type 1 cytoplasmic  
464 envelopment requires functional Vps4. *J Virol*. **81**, 7380–7387 (2007).
- 465 31. F. I. Schmidt *et al.*, Vaccinia virus entry is followed by core activation and  
466 proteasome-mediated release of the immunomodulatory effector VH1 from  
467 lateral bodies. *Cell Rep*. **4**, 464–476 (2013).
- 468 32. S. Gandon, Y. Michalakis, Evolution of parasite virulence against qualitative or  
469 quantitative host resistance. *Proc. Biol. Sci*. **267**, 985–990 (2000).
- 470 33. G. Stack *et al.*, CD200 receptor restriction of myeloid cell responses  
471 antagonizes antiviral immunity and facilitates cytomegalovirus persistence  
472 within mucosal tissue. *PLoS Pathog*. **11**, e1004641 (2015).
- 473 34. R Core Team, “R: A Language and Environment for Statistical Computing” (R  
474 Foundation for Statistical Computing., Vienna, Austria, 2015), (available at  
475 <http://www.R-project.org/>).
- 476 35. R. A. Becker, A. R. Wilks, R. Brownrigg, T. P. Minka, “Maps: draw  
477 geographical maps. R package version 2.3-9” (2010).
- 478 36. R. Brownrigg, “Mapdata: Extra Map Databases, R Package Version 2.2-5”  
479 (2013).
- 480 37. M. Meyer, M. Kircher, Illumina sequencing library preparation for highly  
481 multiplexed target capture and sequencing. *Cold Spring Harbor Protocols*.  
482 **2010**, pdb.prot5448 (2010).
- 483 38. N. Wales *et al.*, New insights on single-stranded versus double-stranded DNA  
484 library preparation for ancient DNA. *BioTechniques*. **59**, 368–371 (2015).
- 485 39. M. Carneiro *et al.*, Rabbit genome analysis reveals a polygenic basis for  
486 phenotypic change during domestication. *Science*. **345**, 1074–1079 (2014).
- 487 40. S. Andrews, FastQC: a quality control tool for high throughput sequence data  
488 (2010), (available at <http://www.bioinformatics.bbsrc.ac.uk/projects/fastqc>).
- 489 41. A. M. Bolger, M. Lohse, B. Usadel, Trimmomatic: a flexible trimmer for  
490 Illumina sequence data. *Bioinformatics*. **30**, 2114–2120 (2014).
- 491 42. J. Zhang, K. Kobert, T. Flouri, A. Stamatakis, PEAR: a fast and accurate  
492 Illumina Paired-End reAd mergeR. *Bioinformatics*. **30**, 614–620 (2014).
- 493 43. H. Li, R. Durbin, Fast and accurate short read alignment with Burrows-  
494 Wheeler transform. *Bioinformatics*. **25**, 1754–1760 (2009).
- 495 44. I. M. H. Aaron R Quinlan, BEDTools: a flexible suite of utilities for comparing  
496 genomic features. *Bioinformatics*. **26**, 841–842 (2010).

497 45. A. W. Briggs *et al.*, Patterns of damage in genomic DNA sequences from a  
498 Neandertal. *Proc. Natl. Acad. Sci. U.S.A.* **104**, 14616–14621 (2007).

499 46. H. Jónsson, A. Ginolhac, M. Schubert, P. L. F. Johnson, L. Orlando,  
500 mapDamage2.0: fast approximate Bayesian estimates of ancient DNA damage  
501 parameters. *Bioinformatics*. **29**, 1682–1684 (2013).

502 47. P. Danecek *et al.*, The variant call format and VCFtools. *Bioinformatics*. **27**,  
503 2156–2158 (2011).

504 48. B. S. Weir, C. C. Cockerham, Estimating F-statistics for the analysis of  
505 population structure. *Evolution*. **38**, 1358 (1984).

506 49. B. Schwalb *et al.*, Package “LSD” (2015).

507 50. C. C. Chang *et al.*, Second-generation PLINK: rising to the challenge of larger  
508 and richer datasets. *GigaScience*. **4**, 7 (2015).

509 51. J. K. Pritchard, M. Stephens, P. Donnelly, Inference of population structure  
510 using multilocus genotype data. **155**, 945–959 (2000).

511 52. J. Y. Cheng, T. Mailund, R. Nielsen, Fast admixture analysis and population  
512 tree estimation for SNP and NGS data. *Bioinformatics*. **33**, 2148–2155 (2017).

513 53. S. D. Turner, qqman: an R package for visualizing GWAS results using Q-Q  
514 and manhattan plots, 1–2 (2014).

515 54. K. Soetaert, T. Petzoldt, R. W. Setzer, Solving differential equations in R:  
516 package deSolve. *Journal of Statistical Software* (2010).

517 55. M. M. Rahman, G. McFadden,  
518 Myxoma Virus dsRNA Binding Protein M029 Inhibits the Type I IFN-  
519 Induced Antiviral State in a Highly Species-Specific Fashion. *Viruses*. **9**  
520 (2017), doi:10.3390/v9020027.

521 56. J. Liu *et al.*, Myxoma virus expressing interleukin-15 fails to cause lethal  
522 myxomatosis in European rabbits. *J Virol*. **83**, 5933–5938 (2009).

523 57. F. J. Zemp *et al.*, Treating brain tumor-initiating cells using a combination of  
524 myxoma virus and rapamycin. *Neuro-oncology*. **15**, 904–920 (2013).

525 58. F. Sievers *et al.*, Fast, scalable generation of high-quality protein multiple  
526 sequence alignments using Clustal Omega. *Mol. Syst. Biol.* **7**, 539–539 (2011).

527 59. C. S. Bond, A. W. Schüttelkopf, ALINE: a WYSIWYG protein-sequence  
528 alignment editor for publication-quality alignments. *Acta Crystallogr. D Biol.*  
529 *Crystallogr.* **65**, 510–512 (2009).

530

531 **Acknowledgements:** We thank the Australian Museum, American Museum of  
532 Natural History, Booth Museum of Natural History, Natural History Museum  
533 (London), Museum of Comparative Zoology (Harvard University), Musée des  
534 Confluences, Muséum National d'Histoire Naturelle (Paris), Museum Victoria,  
535 Queensland Museum, Museum of Zoology (University of Michigan), Smithsonian  
536 Institution National Museum of Natural History and all the curators and museum  
537 technicians who generously sampled and provided historical samples. Marie-  
538 Dominique Wandhammer from Musée Zoologique de la Ville de Strasbourg that  
539 helped to track historical French samples. The British Association for Shooting and  
540 Conservation (BASC), Amanda Holroyd, Simon Whitehead and all volunteers that  
541 contributed with modern rabbit samples. Peter Kerr provided rabbit samples from  
542 NSW (Australia) from before RHDV. Peter Elsworth and Will Dobbie contributed  
543 Queensland post-RHDV samples. Colin Crump provided human cells lines expressing  
544 *VPS4*. Rute Fonseca provided valuable advice concerning ancient DNA  
545 bioinformatics. **Funding:** This work was funded by grants from the Programa  
546 Operacional Potencial Humano–Quadro de Referência Estratégica Nacional funds  
547 from the European Social Fund and Portuguese Ministério da Ciência, Tecnologia e  
548 Ensino Superior to M.C. (IF/00283/2014/CP1256/CT0012), to P.J.E. (IF/00376/2015)  
549 and to J.M.A. (SFRH/BD/72381/2010). J.M.A. was supported by a travel grant from  
550 the Middleton Fund (Cambridge) to undertake work in the Centre of GeoGenetics  
551 (Copenhagen), AM was supported by the European Research Council (grant 647787-  
552 LocalAdaptation). FJ was supported by the European Research Council (grant  
553 281668). LL was supported by the European Research Council grant (339941-  
554 ADAPT). McFadden Lab is supported by National Institute of Health (NIH) grant  
555 R01 AI080607. S.C.G. holds a Sir Henry Dale Fellowship, co-funded by the

556 Wellcome Trust and the Royal Society (098406/Z/12/Z). **Competing interests:** None  
557 declared. **Author contributions:** J.M.A, M.C., P.E., N.F., and F.M.J. designed and  
558 led the study. J.M.A, P.F.C., N.W., S.A., J.P.D and M.T.P.G. generated sequencing  
559 data. J.M.A., T.S., D.J.B, S.J.F, S.M., W.J.P., G.Q., A.K.S. did fieldwork and  
560 extracted DNA. A.L.M., M.M.R, S.C.G., L.B. and G.M., performed the experiments  
561 in cell culture. J.M.A., M.C., J.Y.C., L.L., A.E., A.M., F.G.V., R.N., and F.M.J.  
562 analysed the data. J.M.A., M.C. and F.M.J. wrote the paper with input from the other  
563 authors. All authors approved the manuscript before submission. **Data and materials**  
564 **availability:** Original sequence data are available in the Sequence Read Archive  
565 ([www.ncbi.nlm.nih.gov/sra](http://www.ncbi.nlm.nih.gov/sra)) under BioProject PRJNA393806 (SRP118358). The  
566 variant calls are available in the Cambridge Data Repository  
567 (<https://doi.org/10.17863/CAM.35707>). French modern samples are available from  
568 S.M. under a material agreement with Office national de la chasse et de la faune  
569 sauvage.



**Fig. 1 – Rabbit origins and sampling locations.** Historical (circles) and modern (triangles) sampling locations. Dates in red inside the maps show the date of the first myxomatosis outbreak in the respective countries. Orange dashed arrows and dates reflect historical and archaeological records of the colonisation of European rabbits from France to the United Kingdom and Australia.

**Fig. 2 – Genetic structure and diversity in historical and modern populations of France, United Kingdom and Australia** (a) Principal components analysis (PCA). Ellipses show 95% confidence intervals. (b) Ancestry fractions inferred with Ohana structure analysis for  $K=2$  (top) and  $K=3$  (bottom). Each bar shows the inferred ancestry fraction for an individual. Black lines between bars separate populations. Labels above bars identify country and labels below bars identify temporal set and sample size. Individuals are ordered geographically within each population. (c) Decay of linkage disequilibrium for each population. Each dot represents the averaged pairwise  $R^2$  values between pairs of SNPs in non-overlapping 500bp windows. Colours represent different populations. (d) Expected heterozygosity for each population. The bars are the mean across chromosome arms, and error bars are 95% bootstrap confidence intervals from resampling chromosome-arms. Colours represent different populations. (e) The correlation between the frequency of the alternative allele in historical and modern populations for France, the UK and Australia. Colours reflects the relative density of points according to the scale on the bottom right of each plot, from darker (more density) to lighter (less density).

**Fig. 3 – Parallel changes in allele frequency across three countries.** (a) Venn diagram showing the overlap of the 1000 SNPs with the highest changes in allele frequency between modern and historical samples ( $F_{ST}$ ) in France, the UK, and

Australia. Numbers in black show the observed number of SNPs and numbers in red show the expected overlap after 1000 random permutations of modern and historical samples within each country. **(b)** Scaled histogram of the  $F_{ST}$  values in the three countries. Bars with dark colours reflect SNPs that are in the top 1000 in both of the other two countries. Bars with light colours are SNPs that are in the top 1000 of only one of the other countries. Grey bars are all the remaining SNPs. **(c)** Genome-wide selection scan based on allele frequency changes after the introduction of myxomatosis. (supplementary methods, Equation 5; the strength of selection in each population is allowed to vary independently) **(d)** Selection scan testing whether selection has acted in all three populations (positive values) or just one population (negative values; supplementary methods, Equation 6). **(c and d)** Y-axis shows likelihood ratio statistic of each model. Orange dotted line shows genome-wide 95% significance threshold from permuting sample collection dates within each country. Shaded boxes show SNPs located in the highlighted genes. Different shades of blue show chromosomes. **(e)** Mean of the posterior distribution of the derived allele frequency as a function of time for the *IFN- $\alpha$ 21A* and *FCRL3* loci from the Bayesian selection analysis (additive model). 95% credible intervals are shaded. Triangles across the bottom represent years of samples (only samples post-1940 are shown). Dotted lines show dates of first reports of MYXV and RHDV. List of the top 1000 SNPs for all figures is available in Files S2, S3, and S4.

**Fig. 4 – The effect of *IFN- $\alpha$ 21A* and *VPS4* on viral titres.** (a and b) wild-type (*IFN- $\alpha$ 21A*, grey bars) and variant (var*IFN- $\alpha$ 21A*, yellow bars) *IFN- $\alpha$ 21A* were added at different concentrations to cell culture before infection with **(a)** MYXV-M029KO and **(b)** vesicular stomatitis virus (VSV). Viral titre was measured 1-hour post-infection (blue bars) and 24/48 hours post infection (orange bars). Error bars show standard

619 error of the mean. Statistical significance between wild and mutated interferon  
620 treatments was inferred with a Student's *t*-test across three replicate assays (\*  $P<0.05$ ;  
621 \*\*  $P<0.01$ ). **(c)** HEK293 cell lines stably expressing the wild-type isoform of human  
622 VPS4 (wild-type) or a dominant-negative VPS4 (EQ Mutant) under the control of  
623 ponasterone A (PonA). The HEK293 non-transfected cell line (Parental) was included  
624 as an additional control. Cells were either untreated (PonA-) or pre-treated (PonA+)  
625 with 1  $\mu$ M PonA for 20-24 hours and then infected with wild-type MYXV expressing  
626 a red fluorescent protein (vMyx-tdTomato) at a multiplicity of infection (MOI) 10.  
627 The percentage of infected cells (tdTomato+) was assessed by flow cytometry. Error  
628 bars show standard error of the mean. **(d)** Fluorescence microscope images of VPS4  
629 wild-type and VPS4 EQ mutant HEK293 cells pre-treated with PonA (20-24 hours),  
630 48 hours post-infection with vMyx-tdTomato (MOI 10). The live cell images were  
631 taken using an inverted fluorescence microscope at 10x magnification. FFU, focus  
632 forming unit.

633	<b>Supplementary Materials:</b>
634	Materials and Methods
635	Tables S1 to S4
636	Figs. S1 to S7
637	Files S1 to S10
638	References (34-59)



## Supplementary Materials for

### Parallel adaptation of rabbit populations to myxoma virus

Joel M. Alves<sup>1,2,3\*</sup>, Miguel Carneiro<sup>2,4\*</sup>, Jade Y. Cheng<sup>5,6</sup>, Ana Lemos de Matos<sup>7</sup>,  
Masmudur M. Rahman<sup>7</sup>, Liisa Loog<sup>3,8</sup>, Paula F. Campos<sup>6,9</sup>, Nathan Wales<sup>6,10</sup>, Anders  
Eriksson<sup>11</sup>, Andrea Manica<sup>12</sup>, Tanja Strive<sup>13,14</sup>, Stephen C. Graham<sup>15</sup>, Sandra Afonso<sup>2</sup>,  
Diana J. Bell<sup>16</sup>, Laura Belmont<sup>7</sup>, Jonathan P. Day<sup>1</sup>, Susan J. Fuller<sup>17</sup>, Stéphane  
Marchandeu<sup>18</sup>, William J. Palmer<sup>19</sup>, Guillaume Queney<sup>20</sup>, Alison K. Surridge<sup>16</sup>,  
Filipe G. Vieira<sup>6</sup>, Grant McFadden<sup>7</sup>, Rasmus Nielsen<sup>5,6</sup>, M. Thomas P. Gilbert<sup>6,21</sup>,  
Pedro J. Esteves<sup>2,22</sup>, Nuno Ferrand<sup>2,4,23</sup>, Francis M. Jiggins<sup>1\*</sup>

correspondence to: [joel.alves@arch.ox.ac.uk](mailto:joel.alves@arch.ox.ac.uk), [miguel.carneiro@cibio.up.pt](mailto:miguel.carneiro@cibio.up.pt),  
[fmj1001@cam.ac.uk](mailto:fmj1001@cam.ac.uk)

#### **This PDF file includes:**

Materials and Methods  
Tables S1 to S4  
Figs. S1 to S7  
References

#### **Other Supplementary Materials for this manuscript includes the following:**

Files S1 to S10

## Material and Methods

### Sample collection

To understand the genomic changes that occurred in the European rabbit (*Oryctolagus cuniculus*) in response to myxoma virus, we studied historical populations prior to the beginning of the epizootics, and modern populations from the same locations collected more than 50 years after. We focused on three countries where the development of genetic resistance to myxomatosis has been described: Australia, France and the United Kingdom (6). To mitigate confounding effects caused by existing population structure, the study area was restricted to the south of France, south of Great Britain, and southeast of Australia (Fig. 1 and Fig. S1). The map layout with the sample locations points was generated with the *R* suite (34) using the packages *Maps* (35) and *Mapdata* (36). For clarification purposes, the use of the term “country” refers to the country of origin regardless of being an historical or modern population. The use of the term “population” refers to an historical or modern population within a country. Sample code names were attributed based on the type of sample and location. Each sample is designated by a code of four strings of abbreviations connected by an underscore (e.g. M\_AU\_NSW\_bh1). The first string states the sample type (M for modern and H for historical), the second refers to the country of origin (AU for Australia, FR for France and UK for the United Kingdom), the third refers to the state (Australia), department (France) or county (United Kingdom), and the fourth string represents the sample location (e.g. city, village) followed by the sample number (to distinguish samples collected in the same location).

The historical samples were kindly provided by the following 11 Natural History museums: from Australia, the Australian Museum, the Museum Victoria, and the Queensland Museum; from France, the Musée des Confluences and the Muséum National d'Histoire Naturelle; from the United Kingdom, the Booth Museum of Natural History and the Natural History Museum; and finally from the USA, the American Museum of Natural History, the Museum of Comparative Zoology (Harvard University), the Museum of Zoology (University of Michigan), and the National Museum of Natural History (Smithsonian Institution). We obtained samples in the form of bone, skin or residual tissue, belonging to 128 different rabbit specimens and collected between 1865 and 1956 (File S1). Six rabbits were collected shortly after the release of the virus. Excluding these from the analysis does not affect our conclusions. From these, 95 were converted into genomic libraries and sequenced. The remaining 33 samples were excluded due to extreme low DNA yields.

The modern rabbit samples from Australia and France were donated either by private hunters or collaborators in the form of purified DNA or tissue (skin clips or liver). All the rabbit samples from the United Kingdom were donated by private hunters, whose contact was facilitated in most cases by the British Association for Shooting and Conservation (BASC). In this case, liver samples were collected directly in the field and immediately stored in a falcon tube with absolute ethanol and preserved in dry ice. Tissues from all wild rabbits were taken from animals killed for recreation or pest controlling purposes by certified hunters. Therefore, no wild animal has been killed for the purpose of this study and no animal ethics permit was required. When possible, the individual GPS coordinates for each rabbit was taken and animals were sexed by visual inspection. The livers were then stored at -80°C for future DNA extraction. Details for each sample, including sex, location and GPS coordinates

(when available) are provided in File S1. In total, 78 modern rabbit samples (26 for each population), collected between 2002 and 2013, were obtained for this study.

Rabbit samples between 1985 and 1996 from Australia and the UK were provided by collaborators in the form of purified DNA or tissue (liver or blood) (File S1).

#### DNA extraction from historical and modern samples

The DNA extraction of the historical samples was conducted at the ancient DNA facilities of the Centre for GeoGenetics, Natural History Museum, University of Copenhagen. These facilities integrate a set of anti-contamination procedures such as positive pressure rooms, ultraviolet light and laminar flow hoods where all sample handling is undertaken. The DNA extraction protocol was undertaken in small batches of samples, and surfaces were decontaminated with a diluted sodium hypochlorite solution and 70% ethanol before and after each batch.

Two extraction protocols were used according to the type of tissue. For bone, prior to the DNA extraction, the samples were ground manually or with a mikro-dismembrator in case of more compact bone samples. Bone powder was then mixed with 995 µl of 0.5 M EDTA and 5 µl of proteinase K solution (20 mg/ml), and left to incubate overnight at 56°C. The digested sample was then centrifuged at 12,000 rpm for 5 min to form a pellet. The liquid portion was re-concentrated to a volume of 200-250 µl using a 30-kDa cut-off Centricon micron centrifugal filter unit (Millipore, Billerica, MA) and centrifuged at 4,000 rpm. DNA was then purified using MinElute columns (Qiagen MinElute PCR Purification Kit, Qiagen, Hilden, Germany) according to manufacturer's protocol with the following modification: during the



elution step, the spin columns with buffer EB were incubated at 37°C for 15 minutes to increase DNA yields.

For residual dried tissue and skin samples, the hair was removed prior to the digestion to prevent blockage of the spin columns during the extraction process, and samples cut into smaller pieces to optimise the digestion step. The DNA extraction was done with Qiagen DNAeasy Blood and Tissue Kit (Qiagen, Valencia, CA), following manufacturer's protocol with the following modification: during the elution step, the spin columns with Buffer AE were incubated at 37°C for 15 minutes to increase DNA yields.

For modern samples, the genomic DNA was extracted using the Qiagen DNAeasy Blood and Tissue Kit (Qiagen, Valencia, CA), following the manufacturer's protocol. The DNA concentration of each DNA extract was accessed with a Qubit DNA quantification system (Invitrogen, Carlsbad, CA) using Qubit high-sensitivity assay reagents.

### Library Preparation

The libraries for the historical samples were constructed at the ancient DNA facilities of the Centre for GeoGenetics, Copenhagen, Denmark. From the 128 historical samples, a set of 95, for which the DNA extraction was successful, was used to make genomic libraries.

For each sample a total of 21.25 µl of DNA extract was used to construct a double stranded blunt-end Illumina library using NEBNext DNA Sample Prep Master Mix Set 2 (New England Biolabs, E6070). The protocol was followed according to

the manufacturer's instructions with the following modifications. The reaction volume was reduced by a quarter in the end-repair step and by half in the ligation and fill-in steps. The end-repair stage was performed for 30 minutes at 20°C. The ligation reaction was performed for 25 min at 20°C using Illumina-specific adapters specified in Meyer and Kircher (37). For both steps, after the incubation, the reaction was purified through MinElute spin columns and eluted with a Qiagen EB buffer volume of 15 µl in the end-repair step and 21 µl in the ligation step followed by incubation for 15 minutes at 37°C. The final fill-in reaction was done for 20 minutes at 65°C.

To increase library complexity, each library was amplified in two independent PCR reactions that were combined in the end. The following protocol was used for each 100 µl PCR reaction: 12 µl of unamplified library template, 2 U AmpliTaq Gold polymerase (Applied Biosystems, Foster City, CA), 1X AmpliTaq Gold buffer, 2.5 mM MgCl<sub>2</sub>, 0.2 mM dNTPs, 0.2 µM Illumina Multiplexing PCR primer inPE1.0 primer, 0.2 µM Illumina long index primer, 0.4m/mL of Bovine Serum Albumin (BSA), and water for the remaining volume. Cycling conditions were: 95.0°C for 10 min enzyme activation, 8 to 24 cycles of 95.0°C for 30 s, 60.0°C for 1 min, and 72.0°C for 40 seconds, followed by a final extension of 5 minutes at 72°C (number of cycles varied according to each sample and ranged between 8 and 24). The number of required amplification cycles was estimated based on the technique described by Nathan et al (38).

The long index primer contained Illumina standard indices from 1 to 24 and a set of custom indexes were used for barcoding libraries. The PCR product as purified through a single Qiagen MinElute spin column following the manufacturer protocol and eluted in 25 µl EB buffer following a 10 min incubation at 37°C. Following

amplification, libraries tested on Agilent 2100 Bioanalyzer High Sensitivity DNA chip to evaluate the quality and insert size. Library quantification was undertaken using a qPCR KAPA Library Quantification Kit (Kapa Biosystems) according to the manufacturer's instructions.

For all modern samples, individually barcoded libraries were prepared from the purified genomic DNA at TGAC (The Genome Analysis Centre, Norwich, UK) using the KAPA LTP Library Preparation Kit for Illumina platforms (KAPA Biosystems, Boston, USA) and following the manufacturer's protocol. After PCR amplification, the libraries were quantified using qPCR KAPA Library Quantification Kit (KAPA Biosystems, Boston, USA).

#### Capture design, enrichment and sequencing

Exome enrichment was performed with NimbleGen solution-based captures (NimbleGen SeqCap EZ Developer Library, Roche). The technology is based on the development of millions of overlapping 50-105mer probes that cover the target region. The technique consists of hybridising the probes with the genomic libraries, followed by bead capturing of the complex of capture-oligos and genomic DNA fragments, and a final enrichment step of the captured fragments with PCR amplification.

The custom-capture design was based on the coordinates of the gene annotations of the OryCun 2.0 rabbit reference genome (Ensembl release 2.69) (39). In addition to the coding region, we targeted the mitochondrial genome and three regions of the Major Histocompatibility Complex region (MHC) in chromosome 12,

encompassing 1.75 Mb (20,160,00 to 21,060,000; 22,290,00 to 22,560,000; 23,000,000 to 23.580,000). The exact coordinates of targets are available as a BED file in the File S7. The targets of interest were provided to Roche Nimblegen for the final probe design. All overlapping targets were merged to create a contiguous region, and those smaller than 100 bp were padded at both sides to reach a minimum of size of 100 bp in order to increase the capture efficiency.

The capture-enrichment was undertaken in equimolar pools of individual libraries. These pools were made based on the qPCR quantifications and they were composed by either historical or modern samples. For the historical pools, samples were combined according to their insert size to avoid differential capture performance. A total of 21 pools ranging from 6 to 12-plex were made. Exome-capture was performed on each individual pool using a single capture reaction and following the manufacturer's protocol. Due to the unavailability of a rabbit specific reagent for blocking repetitive regions in the genome at the time, the universal SeqCap EZ Developer Reagent Cot-1 DNA was used following the manufacturer's recommendation. The enrichment and capture of 8 pools was conducted at TGAC (Norwich, UK), while the remaining ones at the University of Cambridge.

After capture-enrichment, each pool was independently sequenced in one lane of HiSeq 2000/2500 Illumina machine using 100bp paired-end reads at TGAC (Norwich, UK) and BGI (Beijing Genomics Institute, China). Four of the pools were sequenced twice resulting in a total of 25 lanes of HiSeq.

#### Sanger sequencing of candidate SNPs

To investigate if the most extreme changes in allele frequency observed in our dataset were caused by MYXV or RHDV, we genotyped SNPs in four of the strongest candidate genes/regions (*i.e.* *CD96*, *FCRL3*, *IFN- $\alpha$ 21A*, and MHC region). The genotyping was made only for modern samples, before and after RHDV epizootics, using PCR followed by Sanger Sequencing using the primers described in Table S3. Genotypes are available in File S8.

### Bioinformatics and processing of sequencing data

*FastQC*, version 0.11.2 (40) was used to evaluate the quality of the raw sequences and potential adaptor contamination. *Trimmomatic*, version 0.32 (41) was used to removed low quality bases and adaptor sequences, using the following options: *TRAILING*=15 (cut bases of the end of the read if below a threshold quality of 15), *SLIDINGWINDOW*=4:20 (perform a sliding window trimming, cutting once the average quality within the window falls below a threshold of 20), and *ILLUMINACLIP*=TruSeq3-PE.fa:2:20:10:1:true (remove adapter contamination; the values correspond in order to: input fasta file with adapter sequences to be matched, seed mismatches, palindrome clip threshold, simple clip threshold, minimum adapter length and logical value to keep both reads in case of read-through being detected in paired reads by palindrome mode). The trimming was undertaken exclusively at the 3' end to allow the identification of PCR duplicates (see below). *PEAR*, version 0.96 (42), was used to merge overlapping paired-end reads into single-end reads, allowing any length size of the assembled sequences.

The merged and unmerged sequence reads (fastq files) were aligned independently to the rabbit reference genome OryCun2.0 using *BWA-MEM*, version

0.7.10 (43) with default options with exception of the parameter `-M`, which marks shorter split hits as secondary a requirement for Picard compatibility. The generated SAM files were converted to their binary format (BAM) and sorted by their leftmost coordinates with *SAMtools*, version 0.1.19 (website: <http://samtools.sourceforge.net/>). Read Group information (RG) was added to the BAM files using the module *AddOrReplaceReadGroups* from *Picard Tools*, version 1.126 (<https://broadinstitute.github.io/picard>). The module *MergeSamFiles* in *Picard* was used to merge all BAM files belonging to the same sample, and the module *MarkDuplicates* was used to remove PCR and optical duplicates. Local realignments of reads around indels were performed with *GATK*, version 3.3.0 (<https://www.broadinstitute.org/GATK>) using with the tools *RealignerTargetCreator* (determines suspicious intervals which require realignment), and *IndelRealigner* (runs the realigner over those intervals).

In order to calculate the number of reads mapped on-target we the tool *intersectBed*, from program *BEDtools*, version 2.22.0 (44) was used to intersect each bam file with a BED file containing the interval coordinates of the target regions. The average percentage of reads mapped on-target was 63.64% for historical samples and 50.46% for modern samples. *SAMtools Flagstats* tool was used to obtain metrics for all generated BAM files. *GATK* module *DepthOfCoverage* was used to calculate the coverage on-target with the option “intervals” and a bed file with the capture coordinates as an input. The mean insert size was inferred with the *Picard Tools* module *CollectInsertSizeMetrics*. Sequencing metrics for all samples are available in File S9.

A specific problem is cytosine deamination in historical samples, which

results in an increase of C→T and G→A substitutions, and therefore a higher transition/transversion ratio (45). To mitigate this effect we followed the conventions of ancient DNA research and used a Bayesian approach to model DNA damage in each sample and reduced base quality scores in the sequence reads to account for the effect. The program *MapDamage*, version 2.06 (46), was used to quantify the damage patterns in these samples, followed by downscaling of the quality score of the potential post-mortem damaged bases. We used default options with exception of the number of reads per sample that was down-sampled to 100,000. Non-overlapping paired-end reads were not rescaled since the option for paired-end reads was not integrated in the program. As sites affected by damage-driven mutations would differ between samples, we also removed variants that occurred at a low frequency (minor allele frequency <0.05 across all individuals in the dataset). This resulted in a transition/transversion ratio in the historical populations that was nearly identical to modern populations at ~3.3, and similar to that observed in human exomes (6).

### Variant calling and filtering

To avoid potential issues caused by differential mapping of historical and modern reads due to their different insert sizes, prior to variant calling we filtered out all reads with a mapping quality (MAPQ) below 40. The variant calling was then performed for each individual BAM using the *HaplotypeCaller* tool from *GATK*. Due to computational burden, the variant calling was restricted to the capture-targeted regions with a padding of 300bp around each target. We assumed that the heterozygosity (proportion of sites that are different from the reference genome) was 0.004 based on previous studies (16), and all the remaining parameters were kept as

default. After obtaining individual gVCF files for each sample, a joint genotyping with all historical and modern samples combined was conducted using the tool *GenotypeGVCFs* with default options.

The resulting raw variant calls (VCF file) went through a set of hard filters to remove potential false variants. The following filters were applied:  $QD < 2.0$ ,  $FS > 60.0$ ,  $MQ < 40.0$ ,  $MQRankSum < -12.5$ ,  $ReadPosRankSum < -8.0$ , where  $QD$  is the variant confidence (from the *QUAL* field) divided by the unfiltered depth of non-reference samples;  $FS$  is the phred-scaled p-value using Fisher's Exact Test to detect strand bias (the variation being seen on only the forward or only the reverse strand) in the reads;  $MQ$  is the Root Mean Square of the mapping quality of the reads across all samples;  $MQRankSum$  is the  $U$ -based  $z$ -approximation from the Mann-Whitney Rank Sum Test for mapping qualities (comparing reads with reference bases versus those with that have an alternate allele); and  $ReadPosRankSum$  is the  $U$ -based  $z$ -approximation from the Mann-Whitney Rank Sum Test for the distance from the end of the read for reads with the alternate allele (if the alternate allele is only seen near the ends of reads, this is indicative of error).

After obtaining a final VCF file, we applied a filter based on population genetics theory, where we removed all positions with a significant excess of heterozygotes assuming Hardy-Weinberg equilibrium. This calculation was made independently for modern and historical datasets and all significant variants ( $P < 0.05$ ) inferred for the two datasets were removed. The reasoning for this filter is that variants with excess of heterozygotes are often a signature of a low mappability region where there is a combination of reads correctly and wrongly mapped. Finally, we applied a filter at the genotype level with *GATK* tool *VariantFiltration*, by keeping



only genotypes with a depth of coverage ( $DP$ ) higher or equal to five and a genotype quality ( $GQ$ ) higher than 20.

For all the following analyses, we only used samples with a minimum coverage on-target of 5x, resulting in final dataset of 152 samples, 75 historical and 77 modern samples (File S1). The predicted impact, the name of the gene and sequence ontology term for each variant was determined using *SnpEff*, version 4.1 (2, 17, 18). Human orthologue information, rabbit gene description, and GO Biological Process were inferred using *Better Bunny* online suite, version 2.3 ((19)) (20, 21).

### Population Genetic Analyses

To compare modern and historical populations, we undertook a set of demographic analyses. For these analyses, we generated a stricter dataset consisting of biallelic and autosomal variants that were contained within the original targets and restricted to exons. Additionally, we restricted the analysis to variants that have been called in at least 90% of the individuals across all populations. This latter filter was applied with *VCFtools*, version 0.1.12 (47). This resulted in a total of 220,696 SNPs.

### Weir & Cockerham's $F_{ST}$

We quantified genetic differentiation between modern and historical populations for each country by calculating the Weir & Cockerham's  $F_{ST}$  per individual variant (48) using *VCFtools* (47). The global  $F_{ST}$  values were calculated using the Weir & Cockerham's weighted  $F_{ST}$  estimate as implemented in *VCFtools*. This analysis was restricted to positions with a minimum of 10 individuals for each population and with

a minor allele frequency  $> 0.05$  across all individuals.

To test for parallel evolution we ranked the variants for each country by  $F_{ST}$  value and kept the top 1000 variants. The top 1000 SNPs were then intersected across the three countries to count how many of those are common between two countries and across all countries. The statistical significance of this intersection was assessed by doing 1000 random permutations of historical and modern samples within each country. We randomised historical and modern individuals within each country. We then calculated the  $F_{ST}$  between these mixed populations and took the top 1000  $F_{ST}$  variants. We repeated this process for each country and then intersected the obtained values across the three countries. This process was then repeated 1000 times to generate a null distribution. Only variants that were polymorphic in all three countries were used in this comparison.

### Changes in Allele Frequency

To estimate allele frequency for each variant in each population we took the individual genotypes of each individual and calculated the allele frequency for the reference and alternative allele for each modern and historical population across the three countries. To visualise the changes in allele frequency between historical and modern populations, we plotted the allele frequency of the reference allele of historical against modern populations. For each comparison, we removed all monomorphic variants within each country and only used variants with a minimum of 10 genotypes and a minor allele frequency of 0.05 across all individuals. The plot was generated with *R* software (34) using the `heatscatter` function in the package *LSD* (49).

## Ohana Structure and PCA

To investigate patterns genetic structure, we started by performing a Principal Component Analysis (PCA) analysis with *Plink2*, version 1.02 (50). To further explore the genetic structure we used the Structure model (51) implemented in the *Ohana* tool suite (52). Briefly, *Ohana* was used to infer global ancestry and the covariance structure of allele frequencies among populations. We then modelled the joint distribution of allele frequencies across ancestry components as a multivariate Gaussian and estimated the population tree that is most compatible with the inferred covariance matrix (Fig. S2). For global ancestry and the covariance structure, we analysed  $K$  values ranging from 2 to 8, where  $K$  is the number ancestry components. For each value of  $K$ , we use 32 independent executions with different random seeds, and report the one that reached the highest likelihood. Only variants with a minimum of 10 genotypes and a minor allele frequency of 0.05 across all individuals were used.

## Expected heterozygosity

Expected heterozygosity was inferred for each polymorphic variant in each population, and averaged across all variants. Only variants genotyped for all six populations were used. To mitigate the effect of damage-driven mutations that could increase the number of singletons due to C to T and G to A substitutions, we calculated the heterozygosity only for transversions. To obtain confidence intervals for the mean of the different chromosome arms, we resampled chromosome arms with replacement and recalculated the statistic.

## Linkage Disequilibrium

To obtain an estimate of linkage disequilibrium for each population we calculated all pairwise  $R^2$  values between pairs of SNPs less than 5Mb apart using *Plink2*, version 1.02 (50). Values were then averaged in non-overlapping 500bp windows for plotting. Only SNPs with a minor allele frequency of 0.05 were kept.

### Selection scan comparing modern and historical samples

To detect selection, we use a new method which models allele frequency changes through time and identifies significant changes in allele frequencies using a likelihood ratio test. This method was implemented in a modified version of the software Ohana (this modified version can be obtained J.Y.C upon request). The basic model is based on the standard Structure model, as shown in Eq 1. Let  $g_{ij}$  be the genotype for individual  $i$  in marker  $j$ , coded as 0, 1, and 2, indicating homozygous for the major allele, heterozygous, and homozygous for the minor allele, respectively. Also,  $q_{ik}$  is the proportion of ancestry of the  $k$ 'th ancestry component in the  $i$ 'th individual, and  $f_{kj}$  is the allele frequency of the major allele in the  $k$ 'th ancestry component for the  $j$ 'th marker. Then, the standard log likelihood function is given by:

$$\ln(L) = \sum_i^I \sum_j^J \left( g_{ij} \cdot \ln \left( \sum_k^K (q_{ik} \cdot f_{kj}) \right) + (2 - g_{ij}) \cdot \ln \left( \sum_k^K (q_{ik} \cdot (1 - f_{kj})) \right) \right) \quad (\text{Eq. 1})$$

Here  $I$ ,  $J$ , and  $K$  indicate the total number of individuals, markers, and ancestry components, respectively. We extended this model to take time-labelled data and time-dependent allele frequency changes into account. Each individual,  $i$ , has had the opportunity to change allele frequencies during  $t_i$  time units, indicating the length of time from the emergence of the infection to the time of sampling of individual  $i$ . We then allowed an individual-specific allele frequency,  $f_{kj}^i$  for each marker  $j$  and each

individual  $i$  at each ancestry component  $k$ , and redefine Equation (1) as

$$\ln(L_j) = \sum_i^I \left( g_{ij} \ln \left( \sum_k^K (q_{ik} \cdot f_{kj}^i) \right) + (2 - g_{ij}) \ln \left( \sum_k^K (q_{ik} \cdot (1 - f_{kj}^i)) \right) \right) \quad (\text{Eq. 2})$$

where the individual specific allele frequency now is a function of the time, rescaled by the average sampling time,  $t_{ave}$ , and also depending on a parameter which measures the strength of time-dependent allele-frequency change:

$$f_{kj}^i = \min \left( 1, \max \left( 0, f_{kj}^{\text{est}} + \alpha \cdot \frac{t_i - t_{ave}}{t_{ave}} \right) \right) \quad (\text{Eq. 3})$$

Here  $\alpha \in [-\max(f_j^{\text{est}}), 1 - \min(f_j^{\text{est}})]$  with  $t_{ave} = \sum_i^I t_i / I$ ;  $t_{modern} = t_{max}$  and

$t_{oldest} = 0$ . We used the dates of introduction of the virus as start-of-selection dates, *i.e.* 1952 in France, 1953 in the UK, and 1950 in Australia (2). The parameter  $\alpha$  measures the magnitude of allele frequency changes. We use this basic model to construct three different models that can be used to test hypotheses about time dependent allele frequency change. For each lineage,  $l$ , in a population tree, we can associate a parameter,  $\alpha$ , which measures the allele frequency change on that lineage. In our case, we have three lineages (lineage 1, 2, and 3) with the associated parameters  $\alpha_1$ ,  $\alpha_2$ , and  $\alpha_3$ .

In Model 1 (Fig. S3a and Eq. 4), for each marker  $j$ , we constructed a likelihood ratio test, where we tested the null hypothesis of  $H_0: \alpha_1 = \alpha_2 = \alpha_3 = 0$  against the alternative hypothesis of  $H_A: \alpha_1 = \alpha_2 = \alpha_3 > 0$ .

$$\frac{L(\alpha_1 = \hat{\alpha}, \alpha_2 = \hat{\alpha}, \alpha_3 = \hat{\alpha})}{L(\alpha_1 = 0, \alpha_2 = 0, \alpha_3 = 0)} \quad (\text{Eq. 4})$$

In Model 2 (Fig. S3b and Eq. 5), for each marker we constructed a likelihood

ratio test, where we tested the null hypothesis of  $H_0: \alpha_1 = \alpha_2 = \alpha_3 = 0$  against the alternative hypothesis of  $H_A: \alpha_1 > 0, \alpha_2 > 0, \alpha_3 > 0$ , where each scalar is estimated separately using maximum likelihood.

$$\frac{L(\alpha_1 = \widehat{a}_1, \alpha_2 = \widehat{a}_2, \alpha_3 = \widehat{a}_3)}{L(\alpha_1 = 0, \alpha_2 = 0, \alpha_3 = 0)} \quad (\text{Eq. 5})$$

In Model 3 (Fig. S3c and Eq. 6), for each marker, we constructed a likelihood ratio test, where we tested the null hypothesis of  $H_0: \max\{H_0^1: \alpha_1 > 0, \alpha_2 = \alpha_3 = 0; H_0^2: \alpha_2 > 0, \alpha_1 = \alpha_3 = 0; H_0^3: \alpha_3 > 0, \alpha_1 = \alpha_2 = 0; \}$  against the alternative hypothesis of  $H_A: \alpha_1 = \alpha_2 = \alpha_3 > 0$ .

$$\frac{L(\alpha_1 = \widehat{a}, \alpha_2 = \widehat{a}, \alpha_3 = \widehat{a})}{\max\{L(\alpha_1 = \widehat{a}_1, \alpha_2 = 0, \alpha_3 = 0), L(\alpha_1 = 0, \alpha_2 = \widehat{a}_2, \alpha_3 = 0), L(\alpha_1 = 0, \alpha_2 = 0, \alpha_3 = \widehat{a}_3)\}} \quad (\text{Eq. 6})$$

Manhattan plots with likelihood values from the selection analyses were plotted with the R package qqman (53). We permuted sample collection dates within each country 1000 times and repeated the analyses above, each time retaining the largest likelihood ratio statistic. This gave us a null distribution from which to obtain genome-wide significance.

#### Bayes factor analysis of parallel and population-specific selection

We examined how often a SNP is under population-specific or parallel selection by comparing our selection models using Bayes factors. First, we used the approach described above to analyse data from each of the three populations independently to

detect SNPs that were under selection (genome-wide significance  $<0.05$  from the permutation test). Using the combined dataset of all three populations, we then calculated Bates factors ( $K$ ) in support of selection acting in one ( $K_1$ ), two ( $K_2$ ) or three ( $K_3$ ) populations, where:  $K_2 = \Pr(\text{Data} \mid \text{selection in two populations}) / \Pr(\text{Data} \mid \text{selection in one populations})$ ;  $K_3 = \Pr(\text{Data} \mid \text{selection in three populations}) / \Pr(\text{Data} \mid \text{selection in two populations})$  and  $K_1 = 1 / K_2$ . For a variant initially detected as selected in Population1:

$$\Pr(\text{Data} \mid \text{selection in one populations}) = L(\alpha_1 = \hat{\alpha}_1, \alpha_2 = 0, \alpha_3 = 0) \quad (\text{Eq. 7})$$

$$\begin{aligned} &\Pr(\text{Data} \mid \text{selection in two populations}) \\ &= \frac{L(\alpha_1 = \hat{\alpha}_{1,2}, \alpha_2 = \hat{\alpha}_{1,2}, \alpha_3 = 0)}{2} + \frac{L(\alpha_1 = \hat{\alpha}_{1,3}, \alpha_2 = 0, \alpha_3 = \hat{\alpha}_{1,3})}{2} \end{aligned} \quad (\text{Eq. 8})$$

$$\Pr(\text{Data} \mid \text{selection in three populations}) = L(\alpha_1 = \hat{\alpha}, \alpha_2 = \hat{\alpha}, \alpha_3 = \hat{\alpha}) \quad (\text{Eq. 9})$$

### Bayesian allele trajectory analysis

We used a Bayesian method for inferring the timing and strength of selection from ancient DNA genotypes described in Loog et al. (19), where the likelihood of the data is a function of the frequency curve of the selected allele in the population and is calculated as the product of the probabilities of all observed alleles:

$$L = \prod_i f(t_i)^{x_i} (1 - f(t_i))^{2-x_i} \quad (\text{Eq. 10})$$

Here  $L$  is the likelihood of the data,  $f(t)$  is the derived allele frequency at the time  $t$ ,  $t_i$  is the age of the sample  $i$ , and  $x_i$  is the number of copies of the derived allele observed in sample  $i$ .

We used a standard selection model with dominance  $h$  of the advantageous allele ( $h = 0$ ,  $h=1/2$  and  $h=1$  corresponds to recessive, additive and dominant effect, respectively) and time-dependent selection strength  $s(t)$  to describe the allele frequency trajectories:

$$\frac{df}{dt} = s(t)f(1-f)[h + (1-2h)f], \quad (\text{Eq. 11})$$

where  $f$  is the frequency of the derived allele and  $s$  is the selection coefficient. The initial value for  $f(t)$  is the ancestral frequency ( $f_{\text{ancestral}}$ ). We assume that selection starts at time  $t_{\text{start}}$  and that selection is zero before this time (and, as a consequence, that allele frequency is constant at level  $f_{\text{ancestral}}$ ). To accommodate change in selection through time, we allowed the selection coefficient to change at the time  $t_{\text{change}}$  ( $t_{\text{change}} > t_{\text{start}}$ ). The selection coefficient was held constant at level  $s_1$  until time  $t_{\text{change}}$ , after which it was held constant at level  $s_2$ .

We assumed that selection began (at time  $t_{\text{start}}$ ) with the first appearance of the myxoma virus (i.e. 1950 in Australia and 1953 in the UK), and then changed (at time  $t_{\text{change}}$ ) when the RHDV virus was reported in the early 1990s (1995 in Australia and 1992 in the UK). For each combination of country (Australia and UK), gene (MHC, *IFN-a21A*, *FCRL3* and *CD96*), and dominance model (recessive, additive or dominant), the remaining model parameters ( $f_{\text{ancestral}}$ ,  $s_1$  and  $s_2$ ) were inferred by making a full parameter sweep where we calculated the deterministic allele frequency trajectory for each parameter combination. We assumed a uniform prior for the



ancestral frequency ( $f_{\text{ancestral}}$  in the range  $[0, 1]$  in steps of 0.01), and the two selection coefficients ( $s_1$  and  $s_2$ ). We then calculated the marginal posterior probability density distribution for each parameter by numerically integrating the likelihood of the data over the remaining parameters. In addition, to visualize the inferred allele frequency trajectories, we calculated the posterior distribution of the allele frequency trajectory through time by weighting the allele frequency trajectory of each parameter combination (sampled from their prior distributions) by the likelihood of the data given the parameters (19).

The analysis was implemented in the statistical environment R v. 3.2.2 (34). The R code is available from GitHub (<https://github.com/LiisaLoog/Rabbit-Selection>) and from L.L. upon request. The deterministic allele frequency curves were calculated using the *lsoda* function in the R package *deSolve* v. 1.12 (54).

### Interferon- $\alpha$ 21A assays

We synthesised two N-His6 tagged IFN- $\alpha$ 21A proteins (File S10). The wild type IFN- $\alpha$ 21A protein sequences matches the Oryzun2.0 reference genome. The variant type differs in three non-synonymous mutations at coding sequence position 523 (G to A, Val175Ile), 542 (G to T, Trp181Leu) and 544 (C to A, Gln182Lys). The codon-optimised genes were cloned into the vector pUC57 and expressed in yeast (*Pichia pastoris*) by GenScript HK Limited (Piscataway, NJ, USA), and affinity purified.

Rabbit kidney cell line RK13 was purchased from Sigma, USA (Cat no. 00021715). RK13-E3 (RK13 cells stably expressing Vaccinia virus E3 protein) was cultured as described before (22). The cell lines were cultured in DMEM

supplemented with 10% FBS, 2mM glutamine, and 100µg of penicillin-streptomycin/ml. The cells were maintained at 37°C in a humidified 5% CO<sub>2</sub> incubator. Construction of wild-type MYXV, vMyx-GFP (WT-MYXV expressing GFP under a poxvirus synthetic early/late promoter) and M029 knockout virus, vMyx-M029KO-GFP were described before (22). The construction of vMyx-M029KO-FLuc-tdTomato virus (M029 knockout virus expressing Firefly luciferase under a poxvirus synthetic early/late promoter), and a tandem-dimer tomato red fluorescence protein (Tr-FP) driven by poxvirus p11 late promoter) was described previously (55). vMyx-M029KO-GFP and vMyx-M029KO-FLuc-tdTomato viruses were grown in RK13-E3 cell lines.

RK13 cells were seeded into 48 well plates at  $2 \times 10^4$  cells per well. Next day, individual wells were treated with either IFN- $\alpha$ 21A or varIFN- $\alpha$ 21A. The IFNs were serially diluted 2-fold starting from 4ng/ml in the same DMEM media used for growing cells and added to the wells (200µl per well) replacing the original media. Next day, cells were infected with vMyx-GFP, vMyx-M029KO-GFP, VSV-GFP viruses at a multiplicity of infection (MOI) of 0.01 in the presence of IFNs. One hour after virus adsorption, the media was removed, washed and incubated with the respective IFNs containing media. In case of VSV virus, the incubation was with DMEM media without any IFNs. The progression of GFP-expressing virus infection was monitored using an inverted fluorescence microscope. Cells were harvested 48 hpi by replacing IFNs containing media with regular DMEM media and stored at -80°C until processed. The cells were freeze-thawed at -80°C and 37°C for three times and sonicated for one minute in ice water to release the viruses from the infected cells. vMyx-GFP and vMyx-M029KO-GFP viruses were tittered by serial dilutions using RK13 and RK13-E3 cells respectively. The foci were counted 48 hpi. For VSV,

virus containing media was collected from each well and stored at -80°C until titration was done. VSV was tittered by serial dilutions using RK13 cells and agarose overlay on the infected cells. The VSV plaques were counted after 24 hpi.

RK13 cells were seeded into 48 well plates at  $2 \times 10^4$  cells per well. Next day, the media in each well was replaced with either IFN- $\alpha$ 21A or varIFN- $\alpha$ 21A containing DMEM (200 $\mu$ l per well) after making 2-fold serial dilutions starting from 4ng/ml. After over-night incubation, cells were infected with vMyx-M029KO-FLuc-tdTomato virus at a MOI of 0.01 in the presence of IFNs. After 48 hpi cells were washed with 1x PBS and lysed using 1x cell lysis buffer (Promega, USA) for 20 mins at room temperature. Luciferase assay reagent was added to the lysate and luciferase reading was taken immediately after adding the substrate using a microplate reader.

### VPS4 Assays

Cell lines and viruses: HEK293 cells (Parental) were grown in Dulbecco's Modified Eagle's medium (DMEM, VWR Life Sciences, Radnor, PA, USA) supplemented with 10% FBS (Sigma-Aldrich, St. Louis, MO, USA), 2mM glutamine, 100 U/mL streptomycin, and 100 mg/mL penicillin (Gibco, Thermo Fisher Scientific, Waltham, MA, USA) (complete DMEM). Ecdysone-responsive stable HEK293 cell lines expressing wild-type VPS4 (Wild Type) and dominant-negative VPS4 (EQ mutant) (30) were cultured in complete DMEM supplemented with 400  $\mu$ g/ml Zeocin (Invivogen, San Diego, CA, USA) and 800  $\mu$ g/ml G418 (Caisson Labs, Smithfield, UT, USA). All the cells were maintained at 37°C in a humidified 5% CO<sub>2</sub> incubator. Two myxoma virus constructs, previously described, were used: vMyx- tdTomato, expressing the tandem-dimer tomato red fluorescent protein driven by a synthetic

early/late poxvirus promoter (56) and vMyx-FLuc-tdTomato, expressing firefly luciferase (driven by a synthetic early/late poxvirus promoter) and tomato red (driven by poxvirus p11 late promoter) (57).

Flow cytometry analyses and fluorescence microscopy on HEK293 cells (VPS4): HEK293 Parental, Wild Type and EQ mutant cell lines were seeded into 6-well plates at  $5 \times 10^5$  cells per well. On the following day, cells were treated with and without 1  $\mu$ M ponasterone A (ponA) (Santa Cruz Biotechnology, Dallas, TX, USA). After 20-24 hours, cells were mock treated or infected with vMyx- tdTomato MOI 10. Cells were harvested at 24 and 48 hours post-infection by cell dissociation with trypsin. Before harvesting cells at 48 hours post-infection, fluorescence microscopy was used to capture live images of infected cells (tdTomato+) on a Leica DMI6000 B inverted microscope (LAS X software) at 10x magnification. Sample viability was assessed using the Live/Dead® Fixable Near-IR Dead Cell Stain kit (Molecular Probes™, Thermo Fisher Scientific, Waltham, MA, USA). Infection and cell viability data were collected on a BD LSRFortessa™ flow cytometer with BD FACSDiva software (BD Biosciences, San Jose, CA, USA). Data were analyzed using FlowJo v10 software. A total of three independent experiments was performed, and for each experiment the corresponding time points were collected in duplicate.

Luciferase assay for HEK293 cells (VPS4): HEK293 Parental, Wild Type and EQ mutant cell lines were seeded into 12-well plates at  $1.5 \times 10^5$  cells per well. Next day, cells were treated with and without 1  $\mu$ M ponasterone A (ponA) (Santa Cruz Biotechnology, Dallas, TX, USA). After 20-24 hours, cells were infected vMyx-FLuc-tdTomato at a multiplicity of infection (MOI) of 10. Samples were harvested at 3, 6, 12 and 24 h post-infection by vigorous pipetting, then centrifuged, washed with

1x DPBS and preserved as cell pellets at -80°C until further processing. Before performing luciferase assay, cell pellets were lysed using 1x cell culture lysis reagent (Promega, Madison, WI, USA) for 20 mins at room temperature. Luciferase assay system (Promega, Madison, WI, USA) was used for reporter quantification following manufacturer's recommendations. Each sample was quantified in triplicate and a total of three independent experiments was performed.

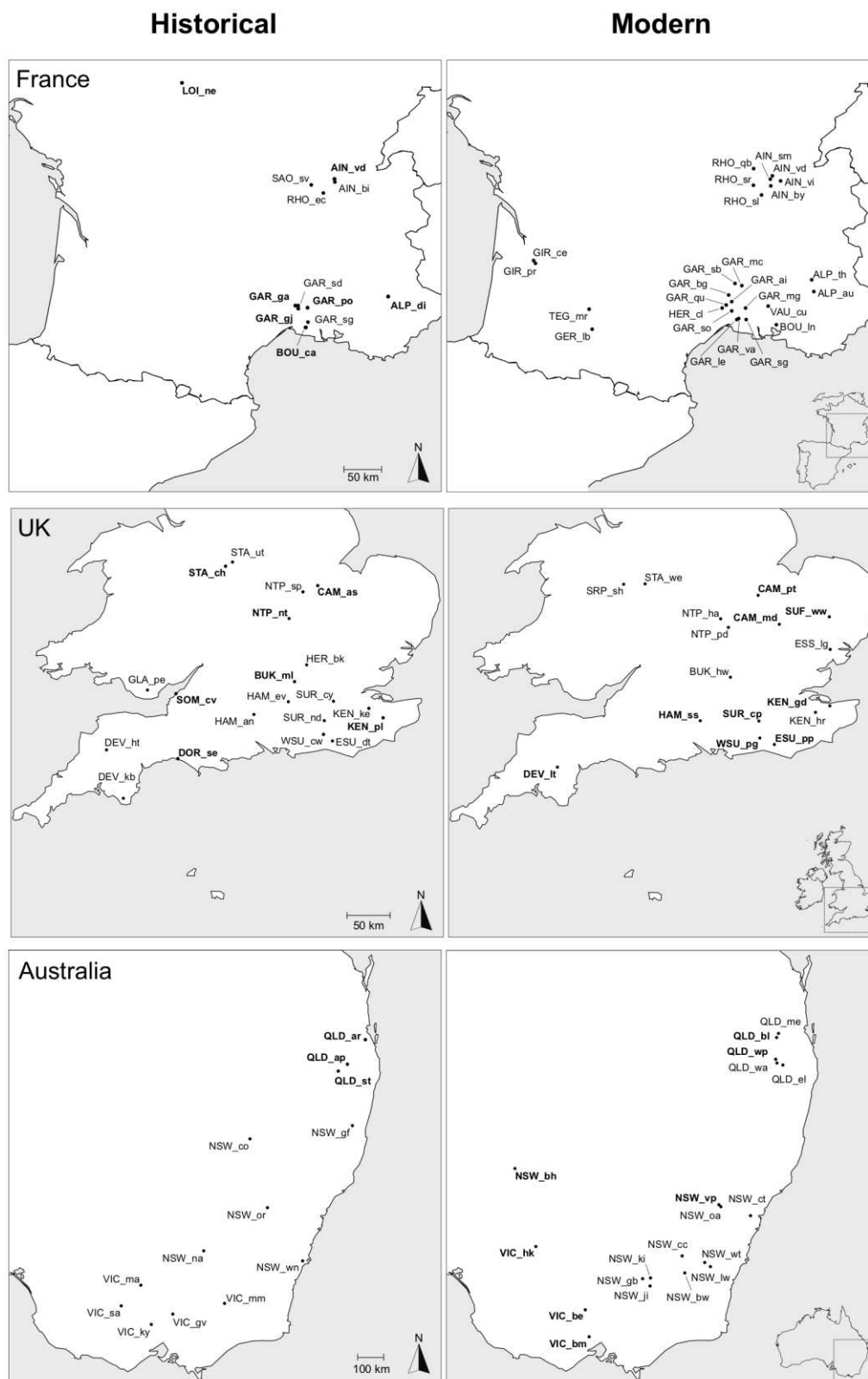
### MFSD1 Assays

Cell lines and viruses: RK13 (European rabbit kidney, BVDV negative) cell line (Sigma-Aldrich, St. Louis, MO, USA) was grown in Dulbecco's Modified Eagle's medium (DMEM, VWR Life Sciences, Radnor, PA, USA) supplemented with 10% FBS (Sigma-Aldrich, St. Louis, MO, USA) and 2mM glutamine (Gibco, Thermo Fisher Scientific, Waltham, MA, USA). Construction of vMyx-FLuc-tdTomato expressing firefly luciferase was described before (Zemp).

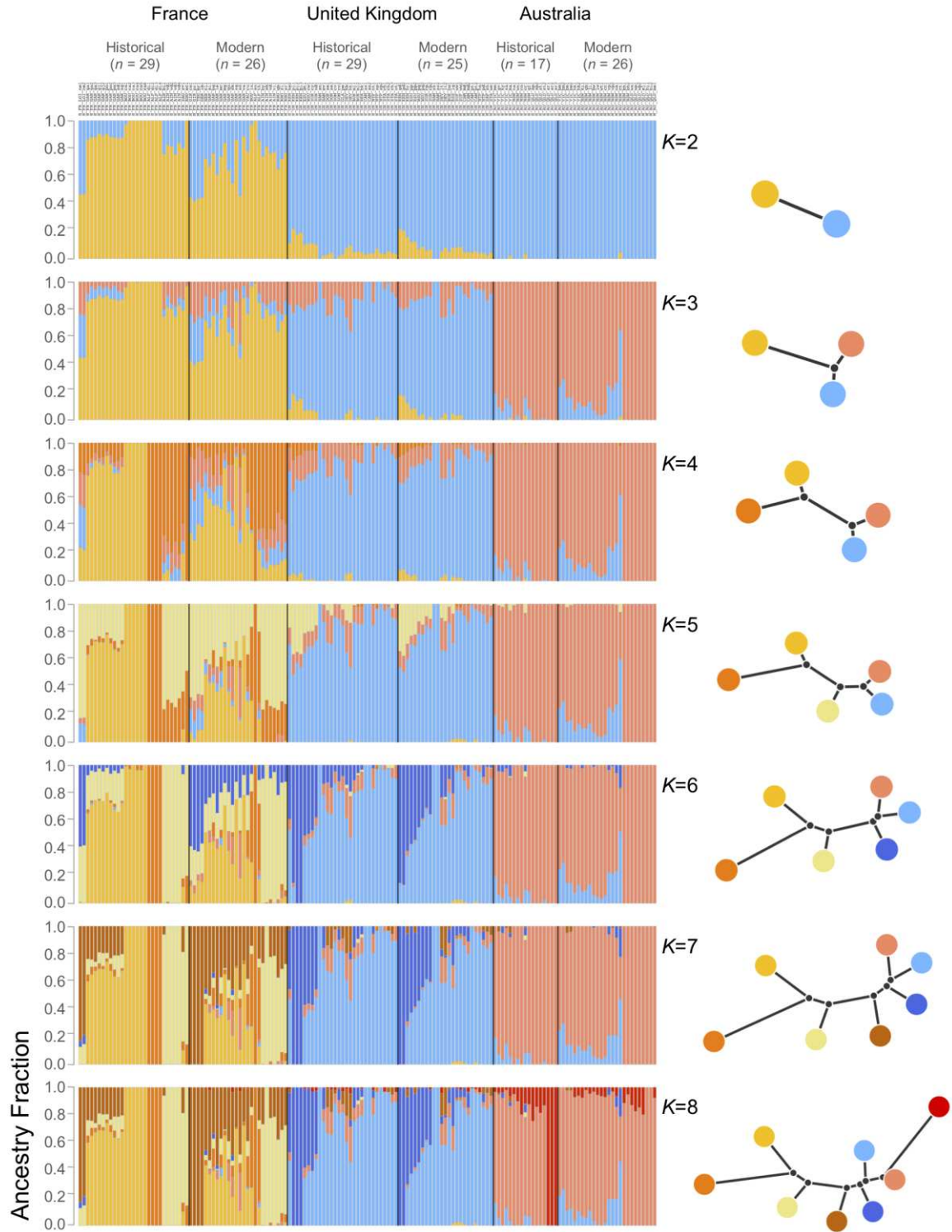
Custom siRNAs were custom designed with dTdT overhang at Dharmacon (United Kingdom. The designs are available in Table S4. siRNA transfection and luciferase assay on RK13 cells (*MFSD1*): RK13 cell line was used to screen for eight different small interfering RNA (siRNA) duplexes targeting European rabbit *MFSD1* (Dharmacon, Lafayette, CO, USA). A functional siRNA against Luciferase was used as a control, FLuc-S1 Positive Control DsiRNA (IDT, Coralville, IA, USA). Cells were plated at 30-40 % confluence per well of a 48-well plate a day before transfection with targeting siRNA, each at a 50 nM concentration, using Lipofectamine RNAiMAX (Invitrogen, Thermo Fisher Scientific, Waltham, MA, USA). After 48 hours, cells were infected with vMyx-FLuc-tdTomato at an MOI 3.

After 1 hour of virus adsorption, cells were washed with 1x DPBS and fresh media was added. At 24 hours post-infection, cells were washed with 1x DPBS and collected by scrapping. Cell pellets were preserved at -80°C until further processing. Later, pellets were lysed using 1x cell culture lysis reagent (Promega, Madison, WI, USA) for 20 mins at room temperature before performing the luciferase assay (Promega, Madison, WI, USA), following manufacturer's recommendations. Each sample was quantified in triplicate and a total of three independent experiments was performed.

*siRNA transfection cytotoxicity on RK13 cells (MFSD1)*: To measure cell viability (cytotoxicity assay) following siRNA transfection, CellTiter 96® AQueous One Solution Cell Proliferation Assay (MTS) was purchased from Promega (Madison, WI, USA). siRNA transfection (adjusted to a 96-well plate), duration and concentration were applied as previously described. After 48 hours of siRNA delivery, the tetrazolium substrate (MTS) was added to RK13 cells and the A490 formazan product that is produced in viable cells was measured using a microplate reader after 1 hour of incubation. Each sample was quantified in triplicate and a total of three independent experiments was performed.



1 **Fig. S1 – Map of sample locations in Australia, France and United Kingdom.**  
2 Maps correspond to our study area for historical (left) and modern (right) samples.  
3 Dots and names show sample locations. Locations in bold have more than one  
4 sample.



6 **Fig. S2 – Ancestry proportions and trees estimates inferred with *Ohana* from**  
 7  **$K=2$  until  $K=8$ .** On the left, ancestry proportions where each bar shows the inferred  
 8 ancestry fraction for an individual. The black lines between bars separate populations.  
 9 Labels on the top identify country, temporal set, sample size and individuals.  
 10 Individuals are ordered geographically within each population. On the right,  
 11 population trees for the ancestry components that are most compatible with the  
 12 inferred covariance matrix for each respective value of  $K$ . Branch length is an  
 13 indication of drift.





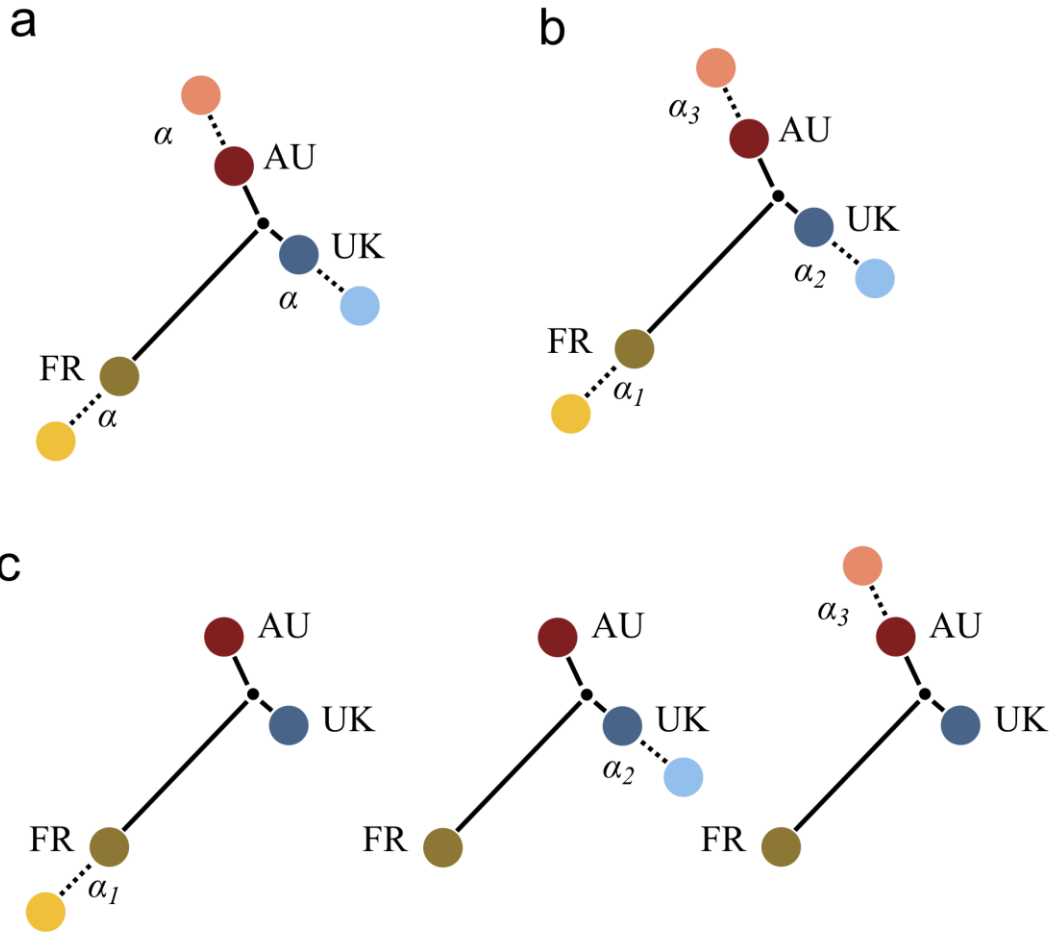


**Fig. S3 – Models implemented in Ohana.** (a). In Model 1, we test the null hypothesis of  $H_0: \alpha_1 = \alpha_2 = \alpha_3 = 0$  against the alternative hypothesis of  $H_A: \alpha_1 = \alpha_2 = \alpha_3 > 0$ . (b). In Model 2, we test the null hypothesis of  $H_0: \alpha_1 = \alpha_2 = \alpha_3 = 0$  against the alternative hypothesis of  $H_A: \alpha_1 > 0, \alpha_2 > 0, \alpha_3 > 0$ . (c). In Model 3, we test the null hypothesis of  $H_0: \max\{H_0^1: \alpha_1 > 0, \alpha_2 = \alpha_3 = 0; H_0^2: \alpha_2 > 0, \alpha_1 = \alpha_3 = 0; H_0^3: \alpha_3 > 0, \alpha_1 = \alpha_2 = 0; \}$  against the alternative hypothesis of  $H_A: \alpha_1 = \alpha_2 = \alpha_3 > 0$ .

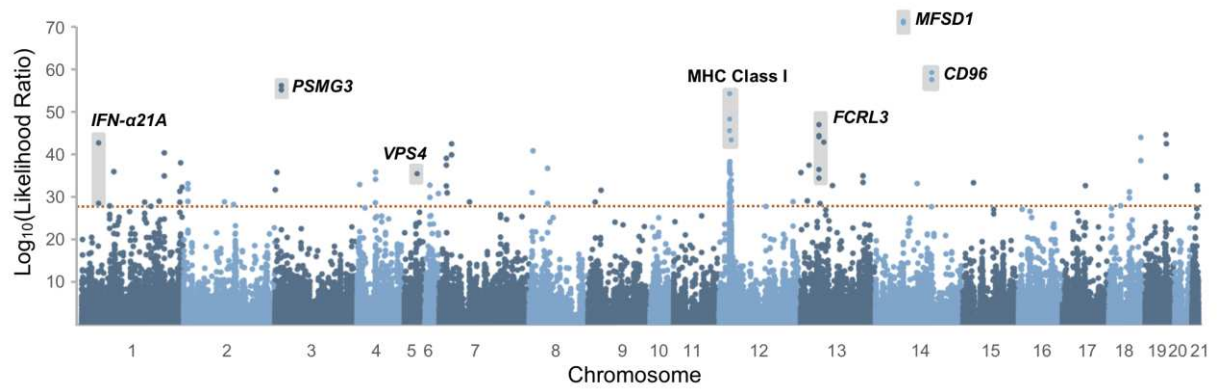


**Fig. S4 – Genome-wide selection scan based on allele frequency changes after the introduction of MYXV.** Selection is assumed to be the same across the three countries (Equation 4, supplementary methods) Y-axis shows likelihood ratio values for the tested model. The orange dotted line shows the genome-wide 95% significance, which was derived by threshold from permuting sample collection dates within each country. Shaded boxes show SNPs located in the highlighted genes. Different shades of blue show chromosomes.

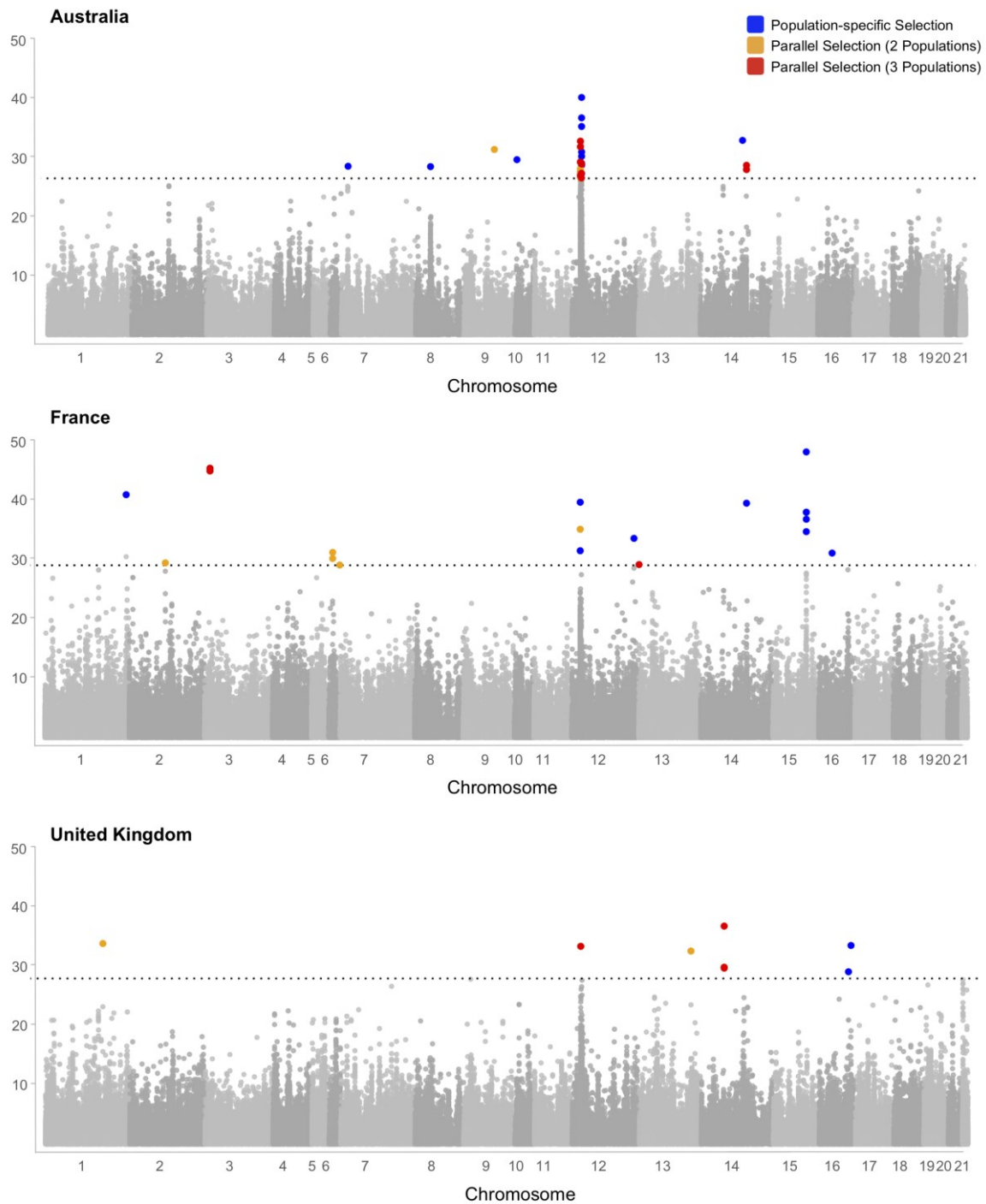


**Fig. S5 - Genome-wide scan for selection in individual populations with SNPs coloured according to evidence of parallelism or population-specific selection.** The horizontal dotted line shows genome-wide 95% significance threshold from permuting sample collection dates within each country. For SNPs above the significant threshold dotted line, those coloured in blue are inferred to be under selection only in that population (Bayes factor  $\geq 3$ ). SNPs coloured in orange and red are inferred to be under selection either in two or the three populations, respectively (Bayes factor  $\geq 3$ ). Different shades of grey show chromosomes. Note all SNPs are shown, not just the most significant SNP per gene.



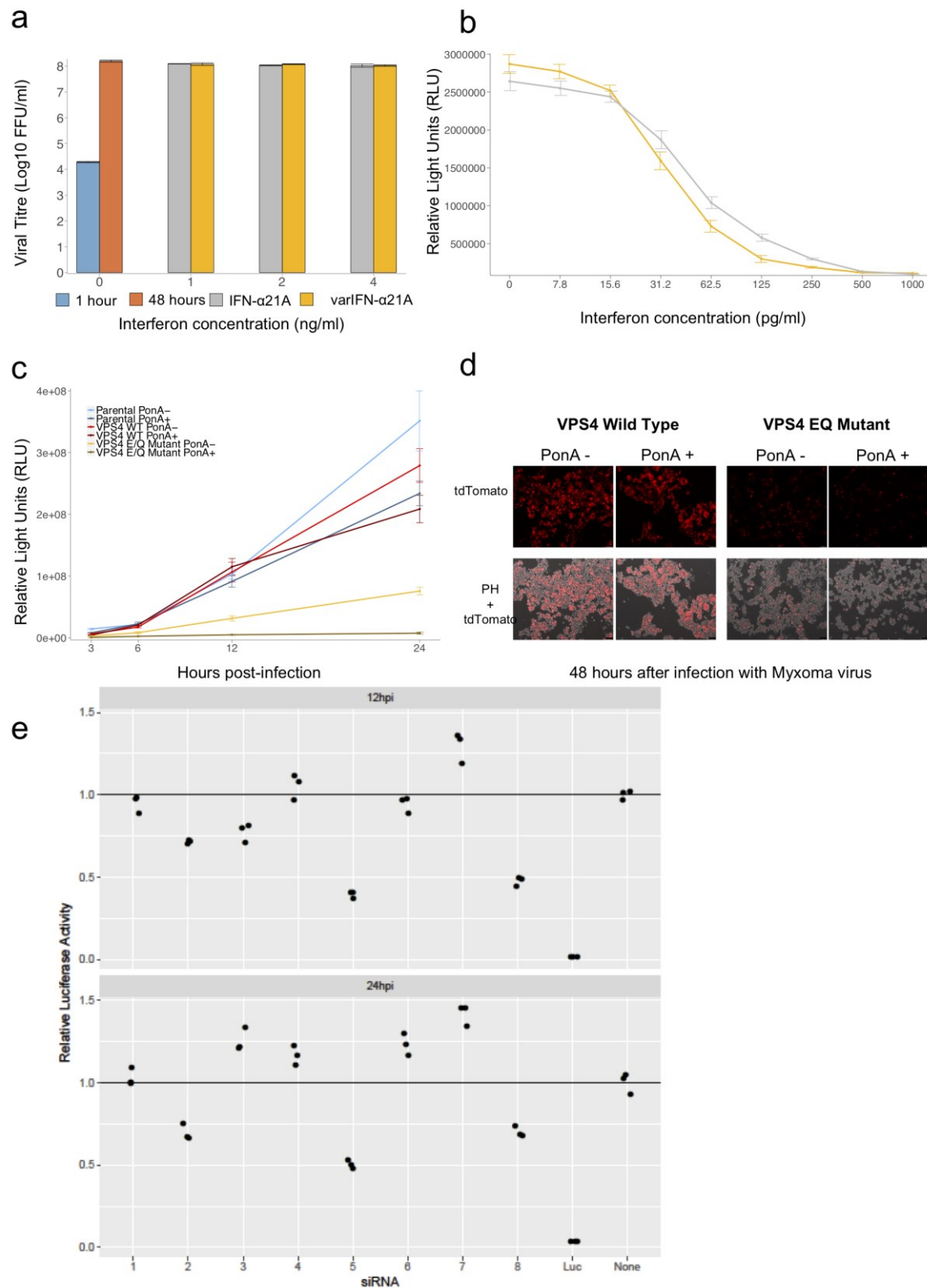


**Fig. S6 – Effect of *IFN- $\alpha$ 21A*, *VPS4* and *MFSD1* on viral titre.** (a) Viral titre measured after 1 hour of infection (blue bars) and after 24/48 hours (orange bars), and after treatment with different concentrations of the wild type IFN- $\alpha$ 21A (grey bars) and variant varIFN- $\alpha$ 21A (yellow bars) for MYXV wild type (vMyx-GFP). Error bars

show standard error of the mean. Statistical significance between wild and variant interferon on viral titer was tested with a Student's t-test across the three replicates (\*  $P < 0.05$ ; \*\*  $P < 0.01$ ). **(b)** Viral gene expression inferred with a luciferase assay for IFN- $\alpha$ 21A (grey bars) and variant varIFN- $\alpha$ 21A (yellow bars) for myxoma virus (vMyx-M029KO-FLuc-TdTomato) at different concentrations. Error bars show standard error of the mean. **(c)** Myxoma virus gene expression on infected HEK293 ecdysone-responsive stable cell lines expressing wild-type VPS4 (Wild Type), dominant-negative VPS4 (EQ Mutant), and on infected control cell line (Parental, no transfection) was evaluated by using a recombinant virus expressing firefly luciferase (vMyx-FLuc-tdTomato). Cells were either kept untreated (PonA-) or pre-treated (PonA+) with 1  $\mu$ M PonA for 20-24 hours, followed by infection at multiplicity of infection (MOI) 10. At 3, 6, 12 and 24 hours post-infection cells were collected and luciferase assay was performed. Error bars show standard error of the mean. **(d)** Fluorescence microscope images of VPS4 Wild Type and EQ mutant HEK293 cells treated with and without PonA (PonA+ and PonA-, respectively), 48 hours after infection with wild-type myxoma virus expressing a red fluorescent protein (vMyx-tdTomato) at MOI 10. Red fluorescence and phase contrast images of live cells were collected 48 hours post-infection using an inverted fluorescence microscope at 10x magnification. **(e)** Effect of MFSD1 on MYXV titre using luciferase. The expression of MFSD1 was knocked down using eight different siRNAs in rabbit RK13 cells. The negative control had no siRNAs, and the positive control had an siRNA against luciferase. Cells were infected with vMyx-FLuc-tdTomato at an MOI 3, and viral titres measured by luciferase fluorescence 24 and 48 hours post infection. The results of three independent biological replicates of each treatment are shown. Viral titres are normalised to the control.

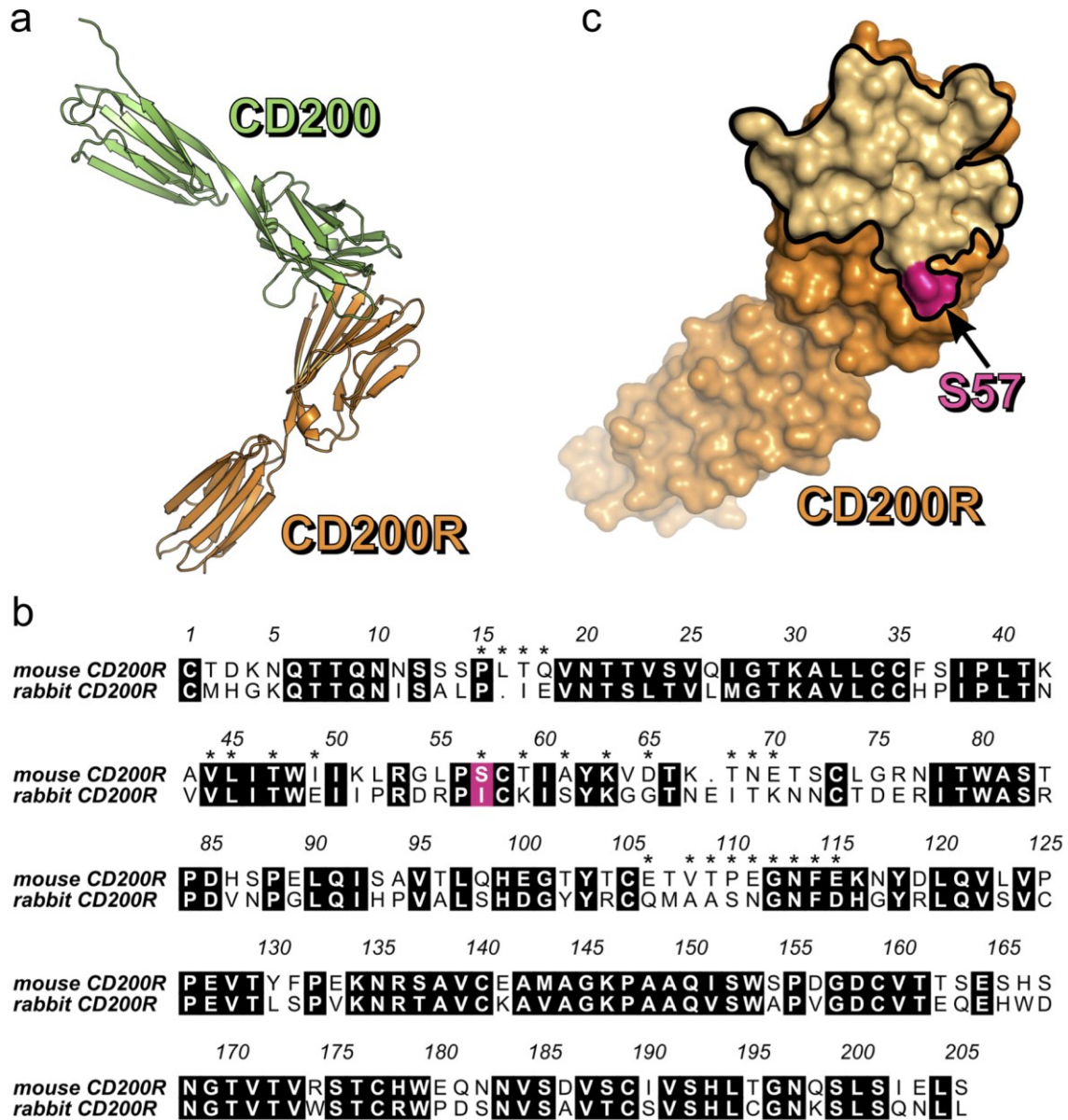


**Fig. S7 – Structure of the CD200:CD200R complex.** (a) The structure of the mouse CD200:CD200R complex (PDB ID 4BFI (23)) is shown as ribbons. Mouse CD200 and CD200R share high sequence identity with their rabbit homologues (78% and 53% across their structured ectodomains, respectively) and the CD200R binding interface of CD200 is strongly conserved across mammals (23), suggesting that the rabbit CD200:CD200R interaction will closely resemble the mouse complex. (b) Sequence alignment of mature mouse and rabbit CD200R. Residues of mouse CD200R that interact with CD200 are starred, and the site of the rabbit CD200R non-synonymous variant (isoleucine to threonine) that is selected in the French population is highlighted. Alignment was generated using Clustal Omega (58) and illustrated using *ALINE* (59) (c) Surface representation of the CD200R, with the CD200-binding interface of CD200R outlined. Mouse CD200R residue S57, equivalent to residue under selection in the French population, is highlighted. Molecular images were generated using *PyMOL* (Schrödinger LLC).



**Table S1** – Global Fixation Index ( $F_{ST}$ ) estimated between population pairs. Only polymorphic loci and a minimum of 10 individual genotypes were used for each two-population comparison.

Comparison	Population 1	Population 2	Variants	Mean $F_{ST}$
Historical versus Modern	France	France	424,922	0.020
	United Kingdom	United Kingdom	466,141	0.009
	Australia	Australia	345,335	0.014
Historical versus Historical	France	Australia	370,971	0.142
	France	United Kingdom	416,041	0.128
	United Kingdom	Australia	367,526	0.067
Modern versus Modern	France	Australia	887,287	0.095
	France	United Kingdom	968,815	0.085
	United Kingdom	Australia	850,659	0.060

**Table S2** – Frequency of the selected allele of SNPs under population-specific selection.

Population selection detected in <sup>1</sup>	<i>N</i>	Mean frequency in Historical Population <sup>2</sup>		
		Australia	France	UK
Australia	9	<b>0.05</b>	0.10	0.12
France	9	0.12	<b>0.07</b>	0.09
United Kingdom	2	0.00	0.00	<b>0.04</b>

<sup>1</sup> Variants were identified as having experienced a significant change in frequency since the release of the myxoma virus (genome-wide  $p < 0.05$  when each population analysed separately) and having evidence for population specific selection (Bayes factor  $> 3$  when comparing a model of selection in 1 population with a model of selection in 2 populations). Within each gene region only the most significant SNP was retained.

<sup>2</sup> The mean frequency of the SNPs among historical samples. The frequency in the population where selection has acted is highlighted in bold

106 **Table S3** – Sanger sequencing primer sequences used for genotyping variants at genes/regions *CD96*, *FCRL3*, *IFN-α21A*, MHC, *PSMG3*.  
107

Gene/Region	Chromosome	Position	Primer Forward	Primer Reverse	Fragment Size (bp)
<i>CD96</i>	14	107622993	GGATCTGTAATGTACTTAAGTGACTGG	GATACTACCCTAATGCAAGGAGTC	158
<i>FCRL3</i>	13	35513450	CTCTGAGGCCCGGACTGT	AGGCCATTGTCAGCCTCA	167
<i>IFNA21A</i>	1	32518812	GCTGTGAGGAAATACTTCCAAGG	CAGGAATCATTTTATGTTGGTCCT	128
MHC	12	20266487	GAGCCTGAGACCTCATCCAG	TG TTCAGAGAGCCCCAACAT	464
<i>PSMG3</i>	3	-	GGACTGCGGGTCTCTTGTC	CACTGCTCCTGTCCTTCACA	429

109 **Table S4** – siRNAs for *MFSD1* gene.

110

siRNA	Chromosome	Position	siRNA (Sense)	siRNA (Antisense)	Target Sequence
<i>MFSD1</i>	14	1278	GUUUGUAGUCCUGAGCAUdTdT	AUGCUCAGGAACUACAAACdTdT	GTTTGTAGTTCCTGAGCAT
<i>MFSD2</i>	14	394	CUGUAUGCCUGGUAUUCUdTdT	AAGAAUACCAGGCAUACAGdTdT	CTGTATGCCTGGTATTCTT
<i>MFSD3</i>	14	628	GUGAGUUGGUUAAAAGGCAdTdT	UGCCUUUAAACCAACUCACdTdT	GTGAGTTGGTTTAAAGGCA
<i>MFSD4</i>	14	955	GUCAUCUGUGUCUGCUAUUdTdT	AAUAGCAGACACAGAUGACdTdT	GTCATCTGTGTCTGCTATT
<i>MFSD5</i>	14	754	GGUUCUGCUGGUCAUACAAdTdT	UUGUAUGACCAGCAGAACCdTdT	GGTTCTGCTGGTCATACAA
<i>MFSD6</i>	14	366	GCAGGUGAAUACCACGAAAdTdT	UUUCGUGGUAUUACCUGCdTdT	GCAGGTGAATACCACGAAA
<i>MFSD7</i>	14	1048	GCAAGUGCAAUUAACAGUAdTdT	UACUGUUAUUGCACUUGCdTdT	GCAAGTGCAATTAACAGTA
<i>MFSD8</i>	14	694	GCAGUACAGUAAACAUGAAdTdT	UUCAUGUUUACUGUACUGCdTdT	GCAGTACAGTAAACATGAA

111

### **Additional Supplementary Material (Separate Files)**

- 112    **File S1** – List of all samples used in this study.
- 113    **File S2** – List containing the top 1000 SNPs based on  $F_{ST}$  for each population.
- 114    **File S3** – List containing the top 1000 SNPs based on *Ohana* (Parallelism).
- 115    **File S4** – List containing the top 1000 SNPs based on *Ohana* (Population-specific).
- 116    **File S5** – Bayes factors for most significant SNP per gene (Population-specific).
- 117    **File S6** – Likelihood ratios and parameter estimation for SNP trajectories over time.
- 118    **File S7** – BED file with probe coordinates for the exome capture.
- 119    **File S8** – Sanger and exome-sequencing genotypes for pre-myxomatosis, pre-RHDV  
120    and post-RHDV samples for four SNPs located at *IFN- $\alpha$ 21A*, *FCRL3*, *CD96* genes  
121    and at the MHC region. Sanger sequencing genotypes of four SNPs, one insertion,  
122    and one deletion, located in *PSMG3* gene for 68 modern individuals from Australia,  
123    France, the UK and the rabbit cell line RK13.
- 124    **File S9** – Sequencing metrics for exome sequencing data.
- 125    **File S10** – Wild type and variant Interferon- $\alpha$ 21A (IFN- $\alpha$ 21A) protein sequences.
- 126

## References:

1. F. Fenner, F. N. Ratcliffe, *Myxomatosis* (Cambridge University Press, Cambridge ; New York, 1965).
2. F. Fenner, B. Fantini, *Biological Control of Vertebrate Pests: The History of Myxomatosis - an Experiment in Evolution*. (CABI publishing, New York, NY, USA, 1999).
3. J. Ross, M. F. Sanders, The development of genetic resistance to myxomatosis in wild rabbits in Britain. *J Hyg (Lond)*. **92**, 255–261 (1984).
4. F. Fenner, J. Ross, in *The European rabbit: The History and Biology of a Successful Colonizer*, H. V. Thompson, C. M. King, Eds. (Oxford University Press, Oxford ; New York, 1994), pp. 205–239.
5. I. D. Marshall, F. Fenner, Studies in the epidemiology of infectious myxomatosis of rabbits. V. Changes in the innate resistance of Australian wild rabbits exposed to myxomatosis. *J Hyg (Lond)*. **56**, 288–302 (1958).
6. P. J. Kerr, Myxomatosis in Australia and Europe: a model for emerging infectious diseases. *Antiviral Res*. **93**, 387–415 (2012).
7. P. J. Kerr *et al.*, Next step in the ongoing arms race between myxoma virus and wild rabbits in Australia is a novel disease phenotype. *Proc Natl Acad Sci USA*. **114**, 9397–9402 (2017).
8. E. M. Veale, The Rabbit in England. *Agric Hist Rev*. **5**, 85–90 (1957).
9. K. Myers, I. Parer, P. Wood, B. D. Cooke, in *The European rabbit: The History and Biology of a Successful Colonizer*, H. V. Thompson, C. M. King, Eds. (Oxford University Press, Oxford ; New York, 1994), pp. 108–157.
10. M. Carneiro, N. Ferrand, M. W. Nachman, Recombination and speciation: loci near centromeres are more differentiated than loci near telomeres between subspecies of the European rabbit (*Oryctolagus cuniculus*). *Genetics*. **181**, 593–606 (2009).
11. L. Kruglyak, Prospects for whole-genome linkage disequilibrium mapping of common disease genes. *Nat Genet*. **22**, 139–144 (1999).
12. A. V. S. Hill, Evolution, revolution and heresy in the genetics of infectious disease susceptibility. *Phil. Trans. R. Soc. B*. **367**, 840–849 (2012).
13. M. M. Magwire *et al.*, Genome-wide association studies reveal a simple genetic basis of resistance to naturally coevolving viruses in *Drosophila melanogaster*. *PLoS Genet*. **8**, e1003057 (2012).
14. J. C. Stephens *et al.*, Dating the origin of the CCR5-Delta32 AIDS-resistance allele by the coalescence of haplotypes. *Am. J. Hum. Genet*. **62**, 1507–1515 (1998).

- 165 15. P. J. Kerr *et al.*, Evolutionary history and attenuation of myxoma virus on two  
166 continents. *PLoS Pathog.* **8**, e1002950 (2012).
- 167 16. J. Abrantes, W. van der Loo, J. Le Pendu, P. J. Esteves, Rabbit haemorrhagic  
168 disease (RHD) and rabbit haemorrhagic disease virus (RHDV): a review. *Vet*  
169 *Res.* **43**, 12 (2012).
- 170 17. H. E. Fuller, D. Chasey, M. H. Lucas, J. C. Gibbens, Rabbit haemorrhagic  
171 disease in the United Kingdom. *Vet. Rec.* **133**, 611–613 (1993).
- 172 18. J. P. Morisse, G. Le Gall, E. Boilletot, Hepatitis of viral origin in Leporidae:  
173 introduction and aetiological hypotheses. *Rev Sci Tech.* **10**, 269–310 (1991).
- 174 19. L. Loog *et al.*, Inferring Allele Frequency Trajectories from Ancient DNA  
175 Indicates That Selection on a Chicken Gene Coincided with Changes in  
176 Medieval Husbandry Practices. *Mol Biol Evol.* **34**, 1981–1990 (2017).
- 177 20. G. L. Smith, J. A. Symons, A. Alcamí, Poxviruses: interfering with interferon.  
178 *Semin Immunol.* **8**, 409–418 (1998).
- 179 21. C. Upton, K. Mossman, G. McFadden, Encoding of a homolog of the IFN-  
180 gamma receptor by myxoma virus. *Science.* **258**, 1369–1372 (1992).
- 181 22. M. M. Rahman, J. Liu, W. M. Chan, S. Rothenburg, G. McFadden, Myxoma  
182 virus protein M029 is a dual function immunomodulator that inhibits PKR and  
183 also conscripts RHA/DHX9 to promote expanded host tropism and viral  
184 replication. *PLoS Pathog.* **9**, e1003465 (2013).
- 185 23. D. Hatherley, S. M. Lea, S. Johnson, A. N. Barclay, Structures of  
186 CD200/CD200 receptor family and implications for topology, regulation, and  
187 evolution. *Structure.* **21**, 820–832 (2013).
- 188 24. D. Hatherley, A. N. Barclay, The CD200 and CD200 receptor cell surface  
189 proteins interact through their N-terminal immunoglobulin-like domains. *Eur.*  
190 *J. Immunol.* **34**, 1688–1694 (2004).
- 191 25. A. L. Hughes, M. Yeager, Natural selection at major histocompatibility  
192 complex loci of vertebrates. *Annu. Rev. Genet.* **32**, 415–435 (1998).
- 193 26. Y. Kochi *et al.*, FCRL3, an autoimmune susceptibility gene, has inhibitory  
194 potential on B-cell receptor-mediated signaling. *J. Immunol.* **183**, 5502–5510  
195 (2009).
- 196 27. L. Martinet, M. J. Smyth, Balancing natural killer cell activation through paired  
197 receptors. *Nat. Rev. Immunol.* **15**, 243–254 (2015).
- 198 28. A. Fuchs, M. Colonna, The role of NK cell recognition of nectin and nectin-  
199 like proteins in tumor immunosurveillance. *Semin. Cancer Biol.* **16**, 359–366  
200 (2006).

- 201 29. G. Sivan *et al.*, Human genome-wide RNAi screen reveals a role for nuclear  
202 pore proteins in poxvirus morphogenesis. *Proc Natl Acad Sci USA*. **110**, 3519–  
203 3524 (2013).
- 204 30. C. M. Crump, C. Yates, T. Minson, Herpes simplex virus type 1 cytoplasmic  
205 envelopment requires functional Vps4. *J Virol*. **81**, 7380–7387 (2007).
- 206 31. F. I. Schmidt *et al.*, Vaccinia virus entry is followed by core activation and  
207 proteasome-mediated release of the immunomodulatory effector VH1 from  
208 lateral bodies. *Cell Rep*. **4**, 464–476 (2013).
- 209 32. S. Gandon, Y. Michalakis, Evolution of parasite virulence against qualitative or  
210 quantitative host resistance. *Proc. Biol. Sci*. **267**, 985–990 (2000).
- 211 33. G. Stack *et al.*, CD200 receptor restriction of myeloid cell responses  
212 antagonizes antiviral immunity and facilitates cytomegalovirus persistence  
213 within mucosal tissue. *PLoS Pathog*. **11**, e1004641 (2015).
- 214 34. R Core Team, “R: A Language and Environment for Statistical Computing” (R  
215 Foundation for Statistical Computing., Vienna, Austria, 2015), (available at  
216 <http://www.R-project.org/>).
- 217 35. R. A. Becker, A. R. Wilks, R. Brownrigg, T. P. Minka, “Maps: draw  
218 geographical maps. R package version 2.3-9” (2010).
- 219 36. R. Brownrigg, “Mapdata: Extra Map Databases, R Package Version 2.2-5”  
220 (2013).
- 221 37. M. Meyer, M. Kircher, Illumina sequencing library preparation for highly  
222 multiplexed target capture and sequencing. *Cold Spring Harbor Protocols*.  
223 **2010**, pdb.prot5448 (2010).
- 224 38. N. Wales *et al.*, New insights on single-stranded versus double-stranded DNA  
225 library preparation for ancient DNA. *BioTechniques*. **59**, 368–371 (2015).
- 226 39. M. Carneiro *et al.*, Rabbit genome analysis reveals a polygenic basis for  
227 phenotypic change during domestication. *Science*. **345**, 1074–1079 (2014).
- 228 40. S. Andrews, FastQC: a quality control tool for high throughput sequence data  
229 (2010), (available at <http://www.bioinformatics.bbsrc.ac.uk/projects/fastqc>).
- 230 41. A. M. Bolger, M. Lohse, B. Usadel, Trimmomatic: a flexible trimmer for  
231 Illumina sequence data. *Bioinformatics*. **30**, 2114–2120 (2014).
- 232 42. J. Zhang, K. Kobert, T. Flouri, A. Stamatakis, PEAR: a fast and accurate  
233 Illumina Paired-End reAd mergeR. *Bioinformatics*. **30**, 614–620 (2014).
- 234 43. H. Li, R. Durbin, Fast and accurate short read alignment with Burrows-  
235 Wheeler transform. *Bioinformatics*. **25**, 1754–1760 (2009).
- 236 44. I. M. H. Aaron R Quinlan, BEDTools: a flexible suite of utilities for comparing  
237 genomic features. *Bioinformatics*. **26**, 841–842 (2010).



238 45. A. W. Briggs *et al.*, Patterns of damage in genomic DNA sequences from a  
239 Neandertal. *Proc. Natl. Acad. Sci. U.S.A.* **104**, 14616–14621 (2007).

240 46. H. Jónsson, A. Ginolhac, M. Schubert, P. L. F. Johnson, L. Orlando,  
241 mapDamage2.0: fast approximate Bayesian estimates of ancient DNA damage  
242 parameters. *Bioinformatics*. **29**, 1682–1684 (2013).

243 47. P. Danecek *et al.*, The variant call format and VCFtools. *Bioinformatics*. **27**,  
244 2156–2158 (2011).

245 48. B. S. Weir, C. C. Cockerham, Estimating F-statistics for the analysis of  
246 population structure. *Evolution*. **38**, 1358 (1984).

247 49. B. Schwalb *et al.*, Package “LSD” (2015).

248 50. C. C. Chang *et al.*, Second-generation PLINK: rising to the challenge of larger  
249 and richer datasets. *GigaScience*. **4**, 7 (2015).

250 51. J. K. Pritchard, M. Stephens, P. Donnelly, Inference of population structure  
251 using multilocus genotype data. **155**, 945–959 (2000).

252 52. J. Y. Cheng, T. Mailund, R. Nielsen, Fast admixture analysis and population  
253 tree estimation for SNP and NGS data. *Bioinformatics*. **33**, 2148–2155 (2017).

254 53. S. D. Turner, qqman: an R package for visualizing GWAS results using Q-Q  
255 and manhattan plots, 1–2 (2014).

256 54. K. Soetaert, T. Petzoldt, R. W. Setzer, Solving differential equations in R:  
257 package deSolve. *Journal of Statistical Software* (2010).

258 55. M. M. Rahman, G. McFadden,  
259 Myxoma Virus dsRNA Binding Protein M029 Inhibits the Type I IFN-  
260 Induced Antiviral State in a Highly Species-Specific Fashion. *Viruses*. **9**  
261 (2017), doi:10.3390/v9020027.

262 56. J. Liu *et al.*, Myxoma virus expressing interleukin-15 fails to cause lethal  
263 myxomatosis in European rabbits. *J Virol*. **83**, 5933–5938 (2009).

264 57. F. J. Zemp *et al.*, Treating brain tumor-initiating cells using a combination of  
265 myxoma virus and rapamycin. *Neuro-oncology*. **15**, 904–920 (2013).

266 58. F. Sievers *et al.*, Fast, scalable generation of high-quality protein multiple  
267 sequence alignments using Clustal Omega. *Mol. Syst. Biol.* **7**, 539–539 (2011).

268 59. C. S. Bond, A. W. Schüttelkopf, ALINE: a WYSIWYG protein-sequence  
269 alignment editor for publication-quality alignments. *Acta Crystallogr. D Biol.*  
270 *Crystallogr.* **65**, 510–512 (2009).

271